

國立交通大學

顯示科技研究所

碩士論文

具高開路電壓之金氧半太陽能電池



MIS Solar Cells with High Open Circuit Voltage

研究生：張鈞隆

指導教授：李柏璵 教授

中華民國九十九年七月

具高開路電壓之金氧半太陽能電池

學生：張鈞隆

指導教授：李柏聰 博士

國立交通大學顯示科技研究所碩士班

摘 要



金氧半太陽能電池的結構中，以氧化層的品質和厚度控制為其重要。我們利用磁控濺鍍機沉積此超薄穿隧氧化層，其厚度由濺鍍的時間控制；薄膜的品質，則由濺鍍的工作壓力以及後續氫退火改善。

首先個別分析 p 型和 n 型的金氧半太陽能電池，一開始以半穿透的金屬薄膜當作載子收集層並且提高開路電壓，為了降低表面反射率及缺陷，我們利用氮化矽或氧化鋁鈦化層分別沉積在具有粗糙化結構的 p 型及 n 型矽基板上，來取代半穿透金屬薄膜。除此之外，鈦化層也會在半導體表面形成反轉層，使得金屬和半導體間獲得更大能障差，進而提高開路電壓。

為了更進一步提升開路電壓，藉由直接晶圓結合的方式將 p 型與 n 型接合形成疊合式金氧半太陽能電池，在標準光源 AM1.5G 的量測系統下，其開路電壓可達到 720mV。

MIS Solar Cells with High Open Circuit Voltage

Student : Chun-Lung Chang

Advisor : Dr. Po-Tsung Lee

National Chiao Tung University

Display Institute

Abstract

In MIS solar cells, the ultrathin insulating layer deposited by radio frequency sputtering plays an important role. Its thickness is controlled by sputtering duration time. The quality of thin film is enhanced by adjusting the working pressure of sputtering and H₂ post-annealing.

The p-type and n-type of MIS solar cells are first investigated. Initially, the semi-transparent metal as a carrier collection layer is used in order to get better open circuit voltage (V_{oc}). Then, both SiN_x and Al₂O₃ are the passivation layers. In order to reduce the surface reflection and defects, SiN_x is deposited on textured silicon substrate of p-type and Al₂O₃ is deposited on that of n-type to replace the semi-transparent metal. In addition, passivation layers can also induce inversion layer at surfaces of semiconductor. The formation makes larger barrier height between the metal and semiconductor and therefore enhances the V_{oc} .

With the aim to further improve the V_{oc} , the p-type and n-type silicon substrates are adhered by the direct wafer bonding technique to form the MIS stacked solar cell. Finally, under the standard measurement AM1.5G, the V_{oc} can reach 720mV.

Acknowledgements

首先，要感謝的就是父母，除了供我讀書之外，還栽培我學習書法，也鼓勵我多參加社團活動，因此豐富了我的求學生涯，另外爺爺、奶奶也常在我回家的時候，給我適時的關心及叮嚀，使我倍感溫馨。

研究所的生活雖然只有短短的兩年，但在這邊學習到，如何在枯燥乏味的實驗中找樂趣？如何在一直失敗的實驗中找到一線生機而不失信心？當然要感謝一起奮鬥的同學們：任勞任怨什麼都好的胖胖、口直心快沒惡意的 YOYO 哥、個性隨和沒生氣過的君源以及一臉正經可嘴上功夫卻是了得的佐哥，雖然我們五位的研究主題都不一樣，但在實驗上都會互相幫忙並給予一些建議。然而實驗室中的學長們更是一群可靠的智囊團：贊文、資岳、明峯、光揚、家揚，沒有你們我的實驗可能要走更多次冤枉路。另外還有一群功不可沒的子弟兵：金剛、文齡、立勛、紹平、雋威、品睿，在我分身乏術之時幫我一把。當然最重要的是謝謝老師您這兩年來，在實驗上不辭辛勞的協助，使我能順利的畢業。最後再一次謝謝 PTLeeLab 的所有成員，包容了我這兩年的任意妄為。

接下來要感謝我的大學同學們，在零星的空閒之餘，能一起開團出遊，調劑一下做實驗的苦悶心情，雖然不像大學時期上山下海那麼瘋狂的遊玩，但這些即興小旅遊，實在是一劑強心針。另外，大學的學弟妹、學長姐們以及朋友們，也要謝謝你們的關心，我研究所可以順利畢業了。最後，特別感謝妳，雖然時間不長，但已經烙印深處，對不起讓妳受委屈，謝謝妳的包容。

這次的結束不僅是新的開始，更是另一個重要的里程碑，不管是人、事、物，我猜想都將變得不一樣，但唯一不變的是，我有這些堅強的回憶當作後盾，繼續支持著我前進。

下一站，社會新鮮人。啟動！

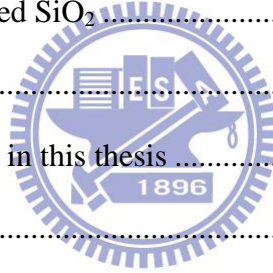
2010/07/14 于新竹 國立交通大學 交映樓 401 室

Content

Abstract (in Chinese)	i
Abstract (in English)	ii
Acknowledgements	iii
Content	iv
List of Tables	vi
List of Figures	vii

Chapter 1 Introduction 1

1.1 Background.....	1
1.2 MIS solar cells	1
1.2.1 MIS-IL solar cells.....	3
1.2.2 Liquid-phase-deposited SiO ₂	6
1.2.3 Anodization SiO ₂	7
1.3 Fabrication of MIS solar cells in this thesis	7
1.4 Thesis organization.....	9



Chapter 2 Characteristics of MIS solar cells 10

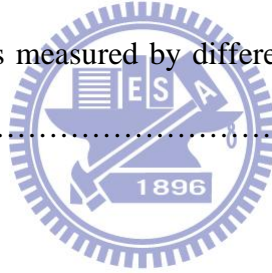
2.1 Photovoltaic properties with SiO ₂ insulating layers	11
2.1.1 The effects of H ₂ annealing	12
2.1.2 The effects of SiO ₂ thickness	15
2.1.3 The effects of working pressure	17
2.2 Photovoltaic properties with different insulating layers.....	20
2.3 Surface texture.....	22
2.4 Surface passivation.....	25
2.5 Photovoltaic properties of p-type MIS solar cells	28
2.6 Photovoltaic properties of n-type MIS solar cells	31

2.7 Summary.....	34	
Chapter 3	MIS stacked solar cells	35
3.1 Tunneling diodes	35	
3.2 Fabrication of MIS stacked solar cells	38	
3.3 Bonding interface by an IR CCD	41	
3.4 Photovoltaic properties of MIS stacked solar cells	44	
3.5 Summary.....	47	
Chapter 4	Conclusion and future work	48
4.1 Conclusion.....	48	
4.2 Future work	49	
References		50



List of Tables

Table 2.1	The key parameters of the MIS solar cells with a ultra-thin sputtering SiO ₂ , PECVD SiN _x , or thermal SiO _x N _y insulating layer.....	21
Table 2.2	Photovoltaic of MIS solar cells after depositing the SiN _x film with non-textured surfaces.....	29
Table 2.3	Photovoltaic of MIS solar cells after depositing the SiN _x film with textured surfaces.....	31
Table 2.4	Photovoltaic of n-type MIS solar cells after depositing Al ₂ O ₃ film or semi-transparent Au.....	33
Table 3.1	Photovoltaic properties of MIS stacked solar cells with and without semi-transparent metal.....	45
Table 3.2	The current density is measured by different measurements (solar simulator and IPCE).....	45



List of Figures

Fig. 1.1	The cross-section of the first generation MIS-IL solar cell with bifacial sensitivity.....	4
Fig. 1.2	Figure of a truncated-pyramid MIS-IL silicon solar cell.....	5
Fig. 1.3	Figure of a wire-grooved Abrased-Ridge-Top solar cell.....	5
Fig. 1.4	Schematic cross-section of the bifacial MIS-n ⁺ p solar cell (MINP).....	6
Fig. 1.5	The structure sketch of (a) n-type MIS solar cell, (b) p-type MIS solar cell....	8
Fig. 2.1	The structure sketch of MIS solar cells.....	10
Fig. 2.2	Photovoltaic properties of p-type MIS solar cell with or without H ₂ annealing.....	13
Fig. 2.3	Photovoltaic properties of n-type MIS solar cell with or without H ₂ annealing.....	13
Fig. 2.4	C-V measurement of p-type MIS solar cell with and without H ₂ annealing.....	14
Fig. 2.5	C-V measurement of n-type MIS solar cell with and without H ₂ annealing.....	14
Fig. 2.6	Thickness dependent J-V curves of p-type MIS	16
Fig. 2.7	Thickness dependent J-V curves of n-type MIS	16
Fig. 2.8	The working pressure dependent J-V curves of p-type MIS solar cells.....	17
Fig. 2.9	The working pressure dependent J-V curves of n-type MIS solar cells.....	18
Fig. 2.10	The working pressure dependent C-V curves of p-type MIS solar cells.....	19
Fig. 2.11	The working pressure dependent C-V curves of n-type MIS solar cells.....	19
Fig. 2.12	SEM image of silicon surface with different etching time: (a) 30 minutes, (b) 40 minutes, (c) 50minutes, (d) 60minutes.....	23

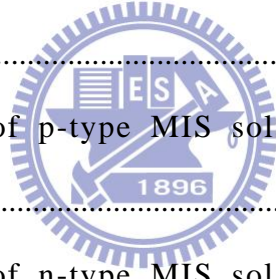


Fig. 2.13	Reflectance of the textured silicon wafers for wavelength between 300 and 1100nm.....	24
Fig. 2.14	Average % reflectance between 300and 1100nm.....	25
Fig. 2.15	Reflectance of the textured silicon wafers after anti-reflection coating for wavelength between 300nm and 1100nm.....	26
Fig. 2.16	Average % reflectance between 300and 1100nm after depositing the SiN _x film.....	27
Fig. 2.17	The structure of p-type MIS solar cells with texture and passivation layer.....	28
Fig. 2.18	Photovoltaic properties of MIS solar cells after depositing the SiN _x film with non-textured surfaces.....	29
Fig. 2.19	Photovoltaic properties of MIS solar cells after depositing the SiN _x film with textured surfaces.....	30
Fig. 2.20	The C-V curve of the SiN _x film with different deposited temperatures.....	31
Fig. 2.21	Photovoltaic properties of n-type MIS solar cells with Al ₂ O ₃ films.....	32
Fig. 2.22	Photovoltaic properties of n-type MIS solar cells with semi-transparent Au.....	33
Fig. 3.1	Schematic energy band diagram and current-voltage property of tunneling diode with varying bias.....	36
Fig. 3.2	The band diagram of the MIS stacked solar cell.....	38
Fig. 3.3	Schematic top view and side view of bonding clamp.....	39
Fig. 3.4	Process flow diagram for the MIS stacked solar cells fabricated.....	40
Fig. 3.5	Schematic diagram of MIS stacked solar cells.....	41
Fig. 3.6	Setup of IR image measurement.....	42
Fig. 3.7	IR images of bonded Si/Si pair in different process Step.....	43

Fig. 3.8 Photovoltaic properties of MIS stacked solar cells with or without semi-transparent metal.....44

Fig. 3.9 IPCE curves of MIS stacked solar cells with and without semi-transparent metal.....46

Fig. 3.10 The transmission of different wafer thickness.....46

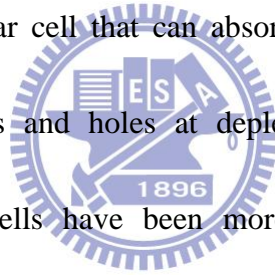


Chapter 1 Introduction

1.1 Background

In a few decades, due to the influences of greenhouse effect and energy crisis, many groups pay much attention on researching and developing other substitute energy. The new energy must be renewable and unpolluted and generate from natural resources such as solar, tides, wind, geothermal heat, hydroelectric and so on. Among those renewable energies, the solar energy plays an important role because it products eternal and enormous energy about $1000\text{W}/\text{m}^2$ without local limitation and pollution.

One of solar energy is the solar cell that can absorb sunlight to convert electrical energy by separating electrons and holes at depletion regions between the p - n junctions. So far, the solar cells have been more promising and potential for worldwide usage.



1.2 MIS solar cells

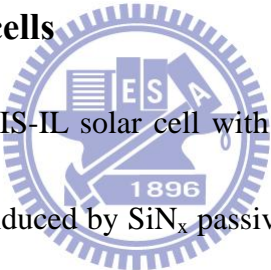
The first solar cell which uses the diffused p - n junction is invented at Bell laboratory in the early 1950's. In that time, the sunlight energy conversion efficiency is about 6%, and the cost is high. Subsequently, the GaAs solar cell with high efficiency is fabricated by Zhore Alferov's group at USSR [1,2]. However, it uses the III-V semiconductor substrates which are so expensive, so the applications of III-V

semiconductor solar cell usually use in outer space. For worldwide usage, the reduction of the cost-per-watt ratio has been a primary issue in solar cell industries.

The formation of $p-n$ junction solar cells needs high thermal budget because diffusion and annealing processes usually carry out about 850°C - 1000°C , and the process are more complex compare with the metal-insulator-semiconductor (MIS) solar cells. Recently, it is has been received much attention on the MIS solar cell because the process are simple and low-temperature fabrication, and the efficiency is comparable to diffused $p-n$ junction solar cells [3-9]. Therefore, MIS solar cells are potential to supersede $p-n$ junction solar cells. The MIS solar cells can be described as a Schottky junction that is fabricated by depositing a thin insulating layer between low work function metal and the p -type semiconductor. There is an electrical filed when Schottky barrier is formed at the surface of semiconductor. Photons generate majority carriers and minority carriers at the Schottky junction, and theses carriers will be driven across the junction from each side, or will be recombined. At the same time, the minority carriers are able to tunnel through insulating layer by quantum mechanism effect while the insulating layer is thin enough [3], and the majority carriers are blocked. However, using the semi-transparent metal layer in MIS solar cell has a major disadvantage that is the metal layer increasing the reflection. In addition, there is a trade-off between carrier collection and surface reflection. To

overcome above issues, grating-type MIS solar cell with only collecting grid fingers is proposed. Although the MIS solar cell has photovoltaic properties, several treatments have been done in order to enhance devices performance. This kind of devices is called an MIS inversion layer (MIS-IL) solar cell [10]. Then, the quality and thickness of insulating layer is also a critical point. Therefore, some reports employ other deposited methods to develop the insulating layer such as the liquid-phase-deposited (LPD) [11] or anodization SiO_2 [12].

1.2.1. MIS-IL solar cells



The cross-section of the MIS-IL solar cell with bifacial sensitivity is shown in Fig 1.1. The inversion layer is induced by SiN_x passivation layer deposited by remote PECVD because of the positive fixed oxide charges a lot in SiN_x film [5]. The SiN_x film covers both the silicon surface and the MIS contacts.

To increase fixed oxide charges in film, the cell has to dip in cesium solution, and cesium ions can easily be caught in the traps [10]. The degradation of cells after cesium dip is faster, so SiN_x layer deposited serves as a passivation layer and decreases the surface recombination [3,10]. In this structure, the ultrathin oxide layer (<2nm) blocks majority carrier (hole) currents injected into the metal at forward bias and reduces surface recombination. Therefore, a higher open circuit voltage (V_{oc}) of

MIS solar cells than that of Schottky barrier solar cells can be achieved.

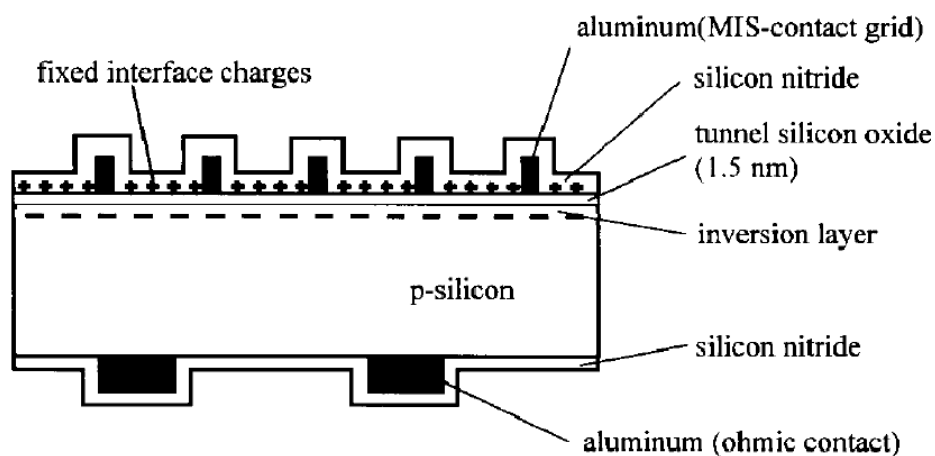


Fig. 1.1: The cross-section of the first generation MIS-IL solar cell with bifacial sensitivity.



However, the surface recombination velocity is still large due to low-temperature SiN_x passivation by PECVD [3,10]. Therefore, the following treatments are applied on MIS-IL solar cells in order to improve the efficiency.

- (a) Formation of truncated-pyramid on semiconductor surface.
- (b) Before front electrodes are deposited, SiN_x passivation layer will deposits at high temperature.
- (c) Selective contact region by window opening on the top after removal of passivation layer.

There are two improved MIS-IL solar cells that are shown in Fig. 1.2 and Fig.

1.3.

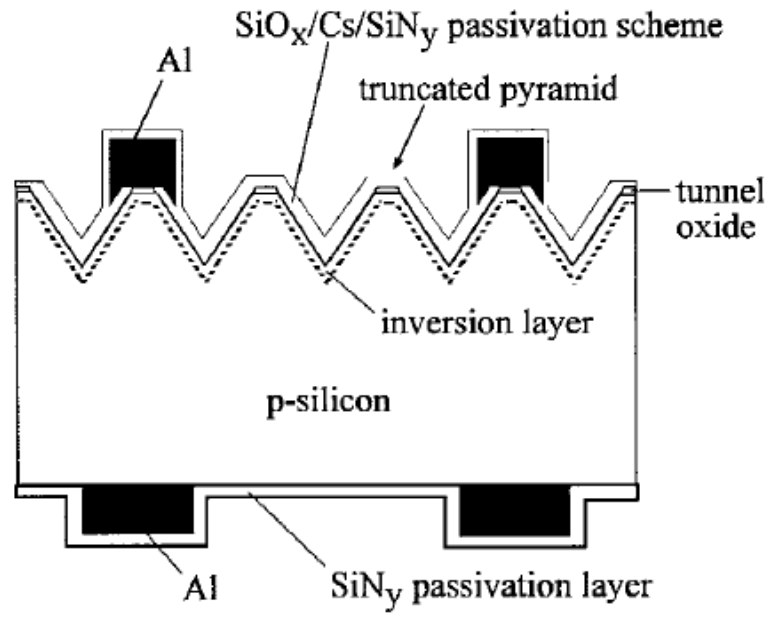


Fig. 1.2: A truncated-pyramid MIS-IL silicon solar cell [13].

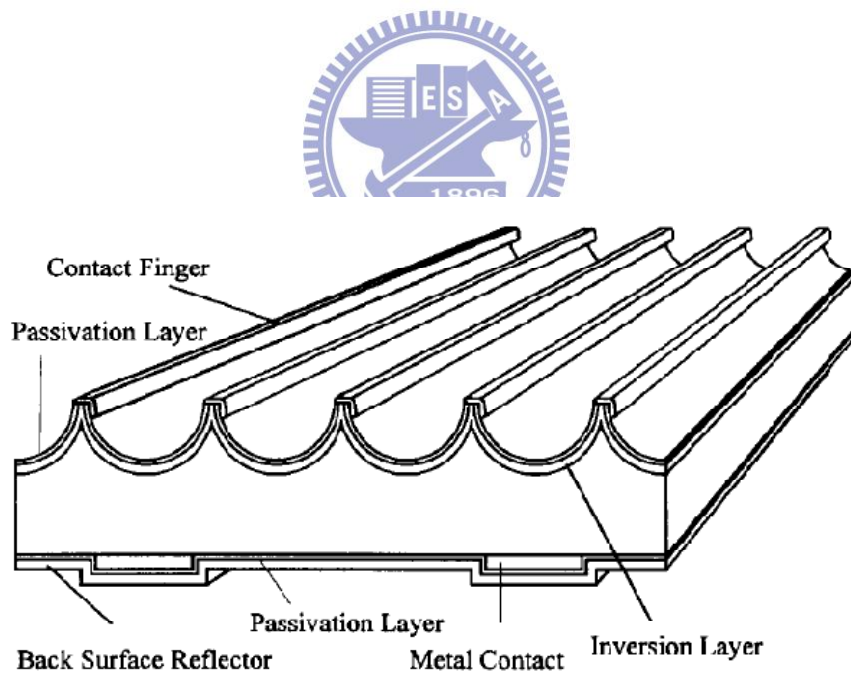


Fig. 1.3: A wire-grooved Abrased-Ridge-Top solar cell [3].

This kind of cells depositing Aluminum electrode on traditional diffused p - n junctions with thin tunneling oxide in between is called hybrid MIS- n^+p [14]. The

MIS-n⁺p structure introduce another *p-n* junction to increase the efficiency, and reduce the surface recombination velocity by the ultrathin tunneling SiO₂. Furthermore, with aluminum in substitution for silver electrode lowers the costs for mass production.

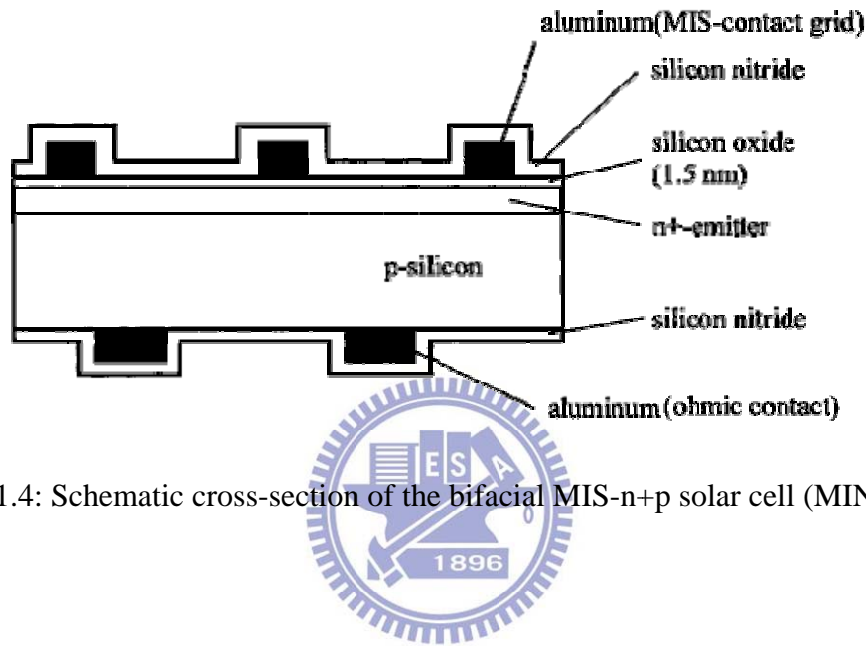


Fig 1.4: Schematic cross-section of the bifacial MIS-n+p solar cell (MINP) [3].

1.2.2. Liquid-phase-deposited SiO₂

The thickness of insulating layer of MIS solar cell must be less than 2nm so that tunneling currents are sufficient for applications. Therefore, how to control the oxide thickness is a challenge. Liquid-phase-deposited (LPD) SiO₂ film is developed to meet the low-temperature requirement with liquid crystal display or electro-luminescent display (ELD) manufacturing [11]. The LPD SiO₂ film is deposited by immersing the substrate in the supersaturated hexafluorosilicic acid (H₂SiF₆) at room temperature. Although the thickness of LPD SiO₂ is up to 7nm, the

current also can tunnel through it by trap-assisted tunneling. All the processes are carried out in room temperature, and the thickness of insulating layer don't need accurately control.

1.2.3. Anodization SiO₂

In order to control oxide thickness, the MIS structure solar cell is prepared by low temperature (<400 °C) anodization technique [12]. The overall reaction of anodization by DI water is listed as below



The silicon substrate is as the anode electrode which is supplied by the positive potential with respect to the Pt cathode electrode during anodization. The Eq. 1.1 shows that chemical reactions of holes accumulated near the p-type substrate. By the anodization time, the thickness of ultrathin insulating layer of MIS solar cell can be controlled appropriately.

1.3 Fabrication of MIS solar cell in this thesis

We employ the semi-transparent metal layer in our MIS solar cell in order to improve the V_{oc} and carrier collection. The detailed processes are listed as below:

- (a) Wafer cleaning with RCA clean

- (b) Deposit the ultrathin silicon dioxide by RF magnetron sputtering
- (c) H₂ annealing at 500°C for 1hr
- (d) Deposit electrodes on the back side by thermal evaporating.
- (e) Deposit a semi-transparent metal on top side of ultrathin oxide by thermal evaporating with shadow mask.
- (f) Deposit finger electrodes on top by thermal evaporating with shadow mask.

The structures of n-type and p-type MIS solar cells are shown in Fig. 1.5



Fig. 1.5: The structures sketch of (a) n-type MIS solar cell, (b) p-type MIS solar cell

1.4 Thesis organization

Even though ultrathin dielectric insulating layers of MIS solar cells using thermal SiO₂, chemical vapor-deposited SiO₂, chemical based SiO₂, or SiO have been demonstrated, it is still difficult to accurately control the thickness of insulating layers.

In this study, we propose the RF magnetron sputtering SiO_2 as the insulating layer of MIS solar cells because the thickness of ultra-thin SiO_2 can be well-controlled by duration time of RF magnetron sputtering. First, the p-type and the n-type MIS solar will be investigated, respectively. Second, the p-type and n-type silicon are adhered by direct wafer bonding technique to form the MIS stacked solar cell.



Chapter 2 Characteristics of MIS solar cells

In this chapter, first, the structure of the MIS solar cell is front electrode/semi-transparent metal/insulating layer/silicon as shown in Fig. 2.1. We focus on researching photovoltaic of both p-type and n-type MIS solar cells with radio-frequency magnetron sputtering SiO_2 as an insulating layer. The sputtering SiO_2 will be investigated into the characteristics of post H_2 annealing, the SiO_2 thickness and the working pressure that affect on performance of MIS solar cells.

Second, the properties of MIS solar cells with a PECVD SiN_x or thermal SiO_xN_y insulating layer are also provided. All devices show similar performance. According to the MIS solar cells using a sputtering SiO_2 insulating layer, it displays simple, low-cost, and low-temperature fabrication process to compare with PECVD SiN_x or thermal SiO_xN_y . Therefore, it suggests that sputtering SiO_2 is a better substitute for insulating layer. Finally, the structure of the MIS solar cell is: passivation layer/front electrode/insulating layer/silicon. Because of the passivation layer, the performance will boost up significantly.

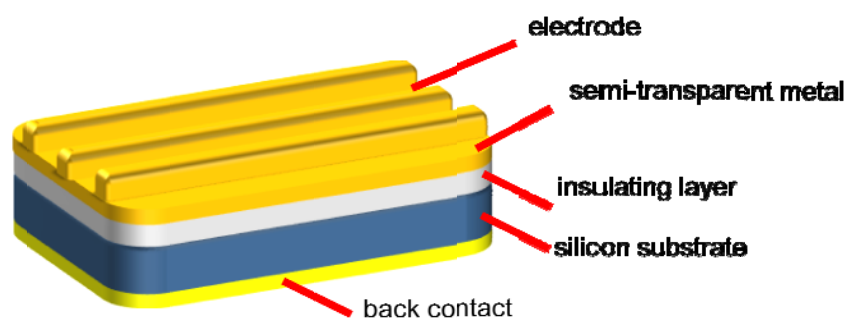


Fig. 2.1: The structure sketch of MIS solar cells.

2.1. Photovoltaic properties with SiO₂ insulating layer

In spite of depositing thermal SiO₂, chemical vapor-deposited SiO₂, chemical based SiO₂, and SiO_x have been used as an ultrathin insulating layer of MIS solar cells. The ultrathin SiO₂ thickness is controlled by sputtering duration. The optimized process conditions of the SiO₂ insulating layer of both high performance p-type and n-type MIS solar cells are obtained. For the p-type MIS solar cell, the SiO₂ insulating layer close to 1 nm is deposited at 20mTorr, and then anneal in hydrogen atmosphere at 500°C for 1 hour as shown in Fig. 2.2 and Fig. 2.3. For the n-type MIS solar cell, the process conditions are the similar to the p-type MIS solar cell, except the thickness of the SiO₂ insulating layer closing to 2 nm.

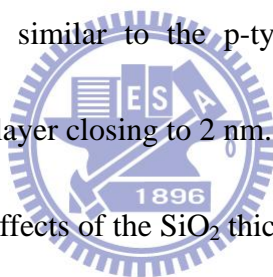


Fig. 2.6 to Fig. 2.9 show effects of the SiO₂ thickness of insulating layer and the working pressure of the sputtering process on the characteristics of MIS solar cells. The different SiO₂ thickness determines the probability for carriers tunneling through the SiO₂. The effects of different working pressure on the SiO₂ quality such as defects and fixed oxide charges are shows in Fig. 2.10 and Fig. 2.11.

2.1.1 The effects of H₂ annealing

The MIS solar cells exhibit poor photovoltaic characteristics without H₂ annealing as shown in Fig.2.2 and Fig.2.3. The interface properties between the ultrathin insulating layers and silicon wafers play an important role in the performance of MIS solar cells. Large leakage current is observed in both C-V curves. It indicates that there are probably a great number of trap states at the interface, such as silicon dangling bonds (i.e., Si dangling bond interface states and suboxide species) and silanol groups [15,16]. Charge carriers can flow via the trap states to cause current leakage, and the capacitance is reduced.

To passivate those traps, H₂ annealing was introduced. Fig. 2.2 to Fig. 2.5 show the *J-V* and *C-V* curves of MIS solar cells with or without H₂ annealing at 500°C for 1 hour. The MIS solar cells with H₂ annealing exhibit better photovoltaic properties. The *C-V* curves of the p-type and n-type MIS solar cells with H₂ annealing display smaller drops at the accumulation region. This can be attributed to the formation of Si-H bonds at the interface. As a result, the trap states can be diminished, and the leakage current is decreased. Therefore, H₂ annealing can improve the performance of MIS solar cells with ultrathin sputtering SiO₂ layers because of the passivation of trap states.

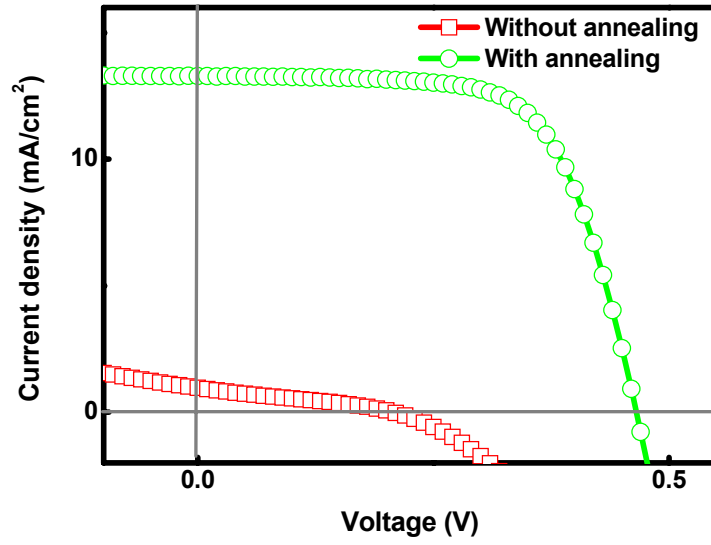


Fig. 2.2: Photovoltaic properties of p-type MIS solar cell with and without H₂ annealing.

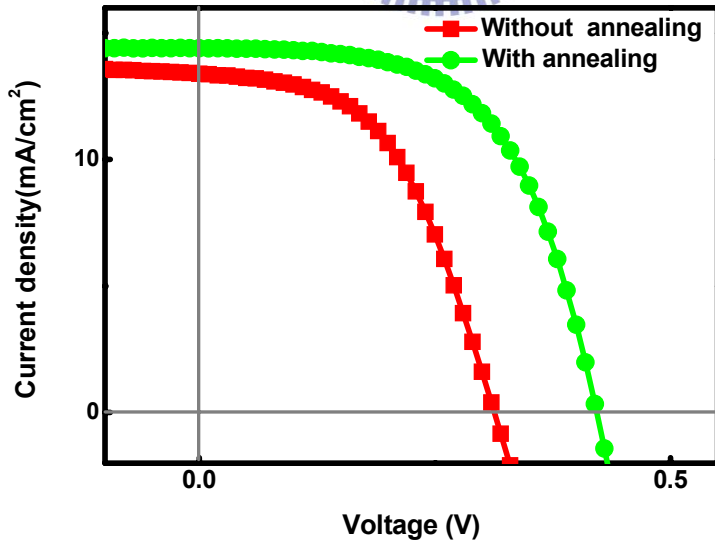


Fig. 2.3: Photovoltaic properties of n-type MIS solar cell with and without H₂ annealing.

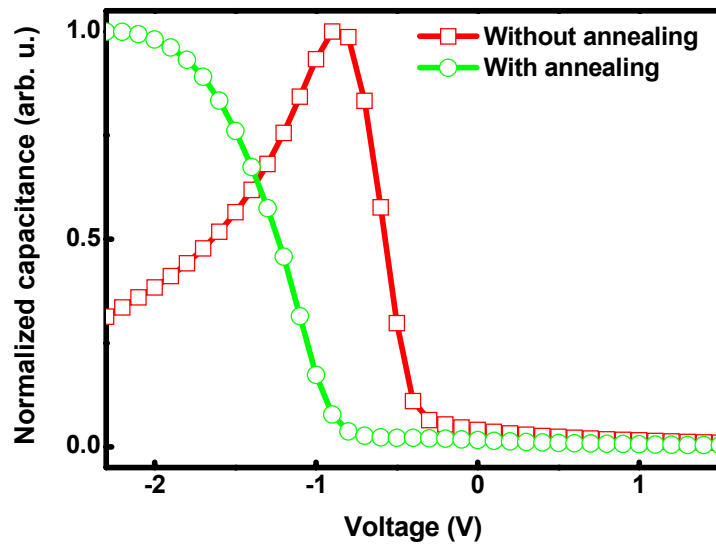


Fig. 2.4: C-V measurement of p-type MIS solar cell with and without H₂ annealing.

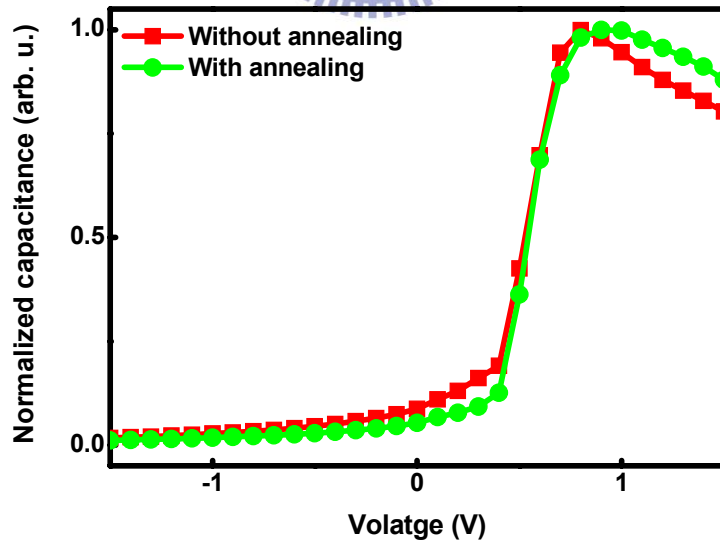
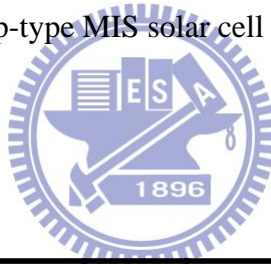


Fig. 2.5: C-V measurement of n-type MIS solar cell with and without H₂ annealing.

2.1.2 The effects of the thickness of SiO₂

The thickness of insulating layer of MIS solar cells must be less than 2 nm so that tunneling currents are sufficient for application. Fig. 2.6 and Fig. 2.7 show the thickness of both p-type and n-type dependent J-V curves of MIS solar cells under AM 1.5G with a SiO₂ insulating layer deposited by RF sputtering. It is obvious that not only V_{oc} but also fill factor (FF) decreased with the increasing thickness of the SiO₂ insulating layer in the p-type MIS solar cells. An ultrathin insulating layer sandwiched between metal and semiconductor can lower carrier recombination probability and thus increases V_{oc} , as shown in Fig. 2.6. But the tunneling probability of minority carriers will be reduced significantly if the thickness of the insulating layer is too thick. As a result, photo-excited carriers can not be collected by electrodes.

Additionally, with increasing thickness, a voltage drop across the insulating layer will also increase, and hence less output power can be used due to thermal dissipation. Therefore, the thickness of the SiO₂ insulating layer plays an important role in the performance of MIS solar cells.

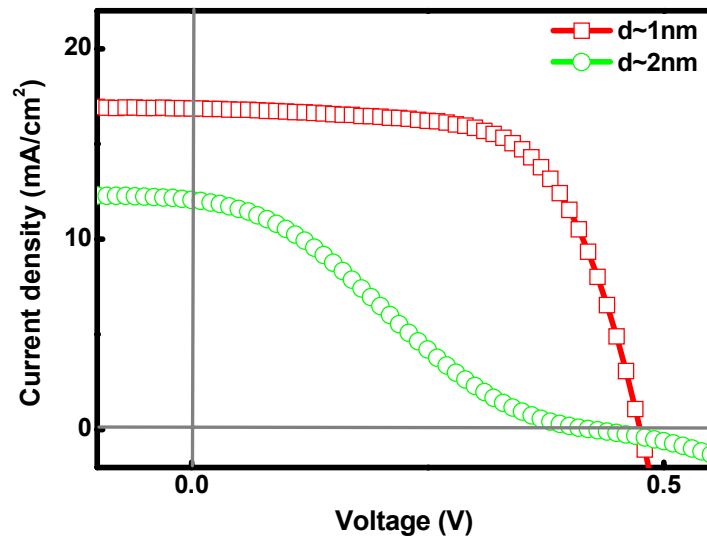


Fig. 2.6: Thickness dependent J-V curves of p-type MIS solar cells.

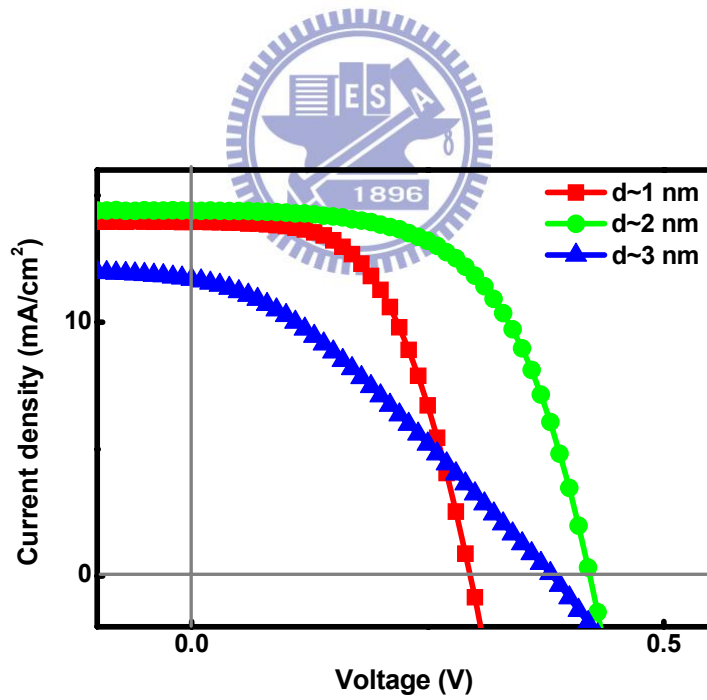


Fig. 2.7: Thickness dependent J-V curves of n-type MIS solar cells.

2.1.3 The effects of working pressure

The J - V curves of the MIS solar cells with the same thickness of ultrathin SiO_2 deposited under different working pressures are shown in Fig. 2.8 and Fig. 2.9 for p-type and n-type respectively. For the p-type MIS solar cells, the V_{oc} values of 475mV, 386mV, and 350mV correspond to working pressures at 20mTorr, 30mTorr, and 40mTorr, respectively. The V_{oc} values of the n-type MIS solar cells are 422mV, 339mV, and 313mV corresponding to working pressures at 20mTorr, 30mTorr, and 40mTorr respectively. Higher working pressure results in lower V_{oc} .

From C - V measurements as shown in Fig. 2.10 and Fig. 2.11, curve shift toward positive bias (Fig.2.10) or negative (Fig. 2.11) with increasing working pressure revealed that the barrier heights at MIS junctions are reduced. Furthermore, the slowly capacitances rise at 30mTorr and 40mTorr marked by the yellow circles of working pressure. Those indicated that more defects are induced in the ultrathin SiO_2 insulating layers with increasing working pressure because of more plasma damages. Therefore, the working pressure of RF magnetron sputtering affects on the barrier height and defect density.

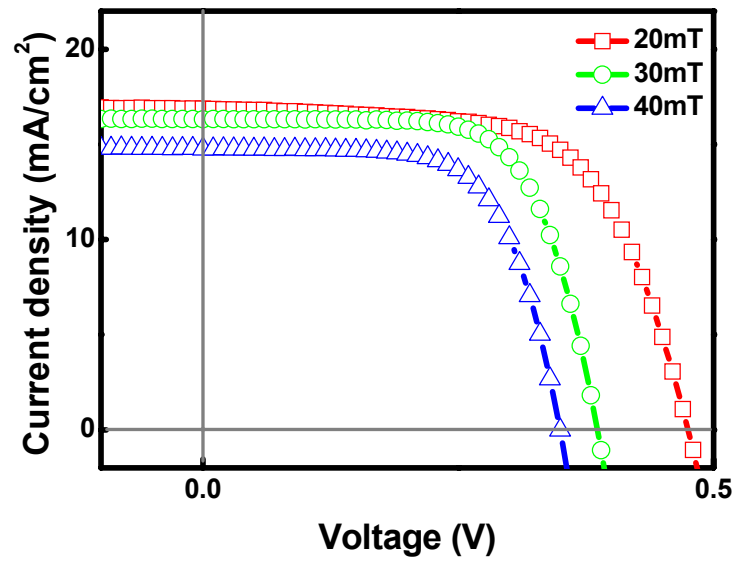


Fig. 2.8: The working pressure dependent J-V curves of p-type MIS solar cells.

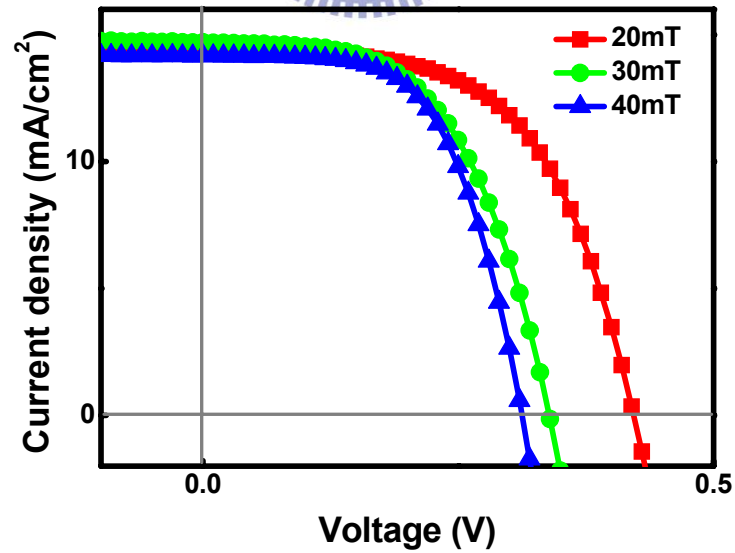
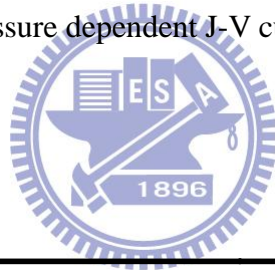


Fig. 2.9: The working pressure dependent J-V curves of n-type MIS solar cells.

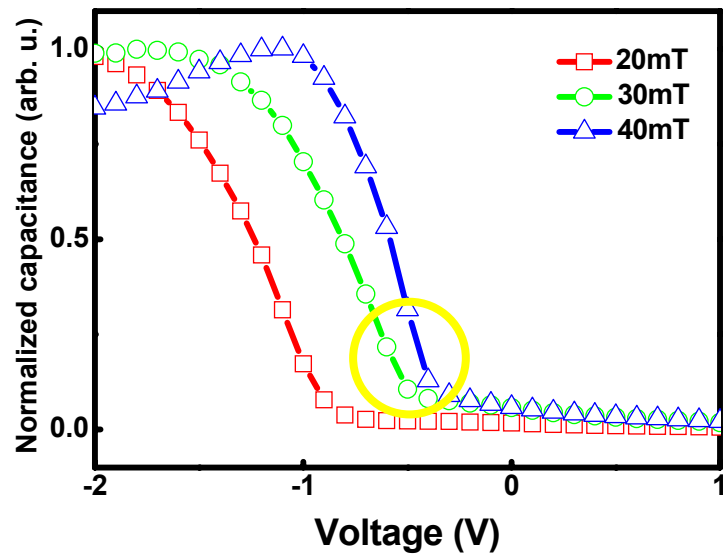


Fig. 2.10: The working pressure dependent C-V curves of p-type MIS solar cells.

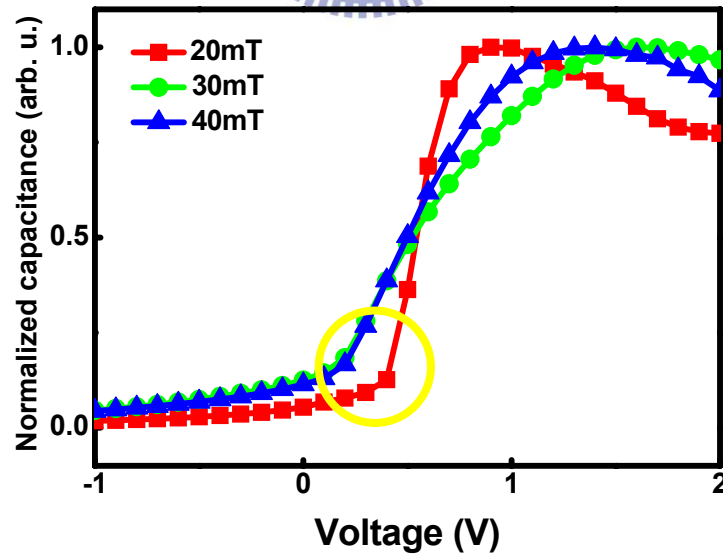
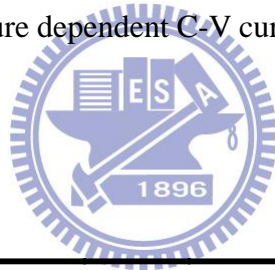


Fig. 2.11: The working pressure dependent C-V curves of n-type MIS solar cells.

2.2. Photovoltaic properties with different insulating layer

The key parameter of MIS solar cells is the insulating layer. In addition to sputtering ultrathin SiO_2 , the insulating layers are deposited by PECVD SiN_x or furnace SiO_xN_y for comparison. The ultrathin SiN_x are deposited by PECVD at 300°C by pyrolysis of silane diluted in Ar (2% SiH_4 in Ar) at a pressure of 100 pa and the rf power at 35w. The ultra thin SiO_xN_y were deposited by quartz furnace at filling with mixing gas oxygen and Nitrous oxide at 500°C .

Table 2.1 lists the important properties of the MIS solar cells with a ultrathin sputtering SiO_2 , PECVD SiN_x , or thermal SiO_xN_y insulating layer. It is obvious that the characteristics with a sputtering SiO_2 insulating layer are comparable to those of the others. If all MIS solar cells were deposited with a passivation layer(s), their performance would be greatly promoted. This is because of the passivation layer(s) can reduce surface recombination rate and the reflection of incident light. In addition, the passivation layer(s) can provide positive or negative charges to induce inversion layers near the surfaces.

From above results, sputtering SiO_2 is an excellent alternative insulating layer of MIS solar cells because of comparable characteristics of that using a PECVD SiN_x or thermal SiO_xN_y insulating layer and better thickness control.

Table 2.1: The key parameters of open circuit voltage, short circuit current density, filling factor, energy conversion efficiency of the MIS solar cells with a ultrathin sputtering SiO_2 , PECVD SiN_x , or thermal SiO_xN_y insulating layer.

Substrate	Insulating layer	$V_{oc}(\text{mV})$	$J_{sc}(\text{mA}/\text{cm}^2)$	FF(%)	$\eta(\%)$
p-type	SiO_2	475	16.9	64.3	5.15
n-type	SiO_2	422	14.4	58.4	3.55
p-type	SiN_x	530	9.07	76.3	3.71
n-type	SiN_x	420	16.50	60.7	4.20
p-type	SiO_xN_y	531	13.35	72.8	5.17
n-type	SiO_xN_y	314	10.26	70.5	2.27

The characteristics of MIS solar cells with sputtering a SiO_2 insulating layer are studied. Influences of the thickness of the SiO_2 insulating layer and the working pressure of the sputtering process are discussed. The thickness of the SiO_2 insulating layer has a great impact on tunneling probability of photo-excited minority carriers, carrier recombination rate, and carrier collection efficiency. The working pressure of RF magnetron sputtering has a significant impact on the barrier height and interface defect density. The sputtering SiO_2 is a good choice as a insulating layer of MIS solar cells due to similar characteristics of that using a PECVD SiN_x or thermal SiO_xN_y insulating layer.

So far, the structure is front electrode / semi-transparent metal / insulating layer / silicon. The reflectance raises because of the semi-transparent metal. Therefore, the

semi-transparent metal will be removed, textured surface will be formed, and then the passivation layer will be deposited on top surface that will be discussed in the next sections.

2.3. Surface texture

Optical and electrical losses are two major reasons that reduce the conversion efficiency of silicon solar cells. Surface texturing is well known as one of the methods to enhance the conversion efficiency of silicon solar cells by increasing the short circuit current through effective light trapping. The textured surfaces of crystalline silicon wafer are usually made in alkaline solutions. Alkaline etching of silicon, such as potassium hydroxide (KOH) [20-22] and sodium hydroxide (NaOH) [17-19], is anisotropic in nature, and therefore representative results of texturing for solar cell is forming random pyramids on the surface.

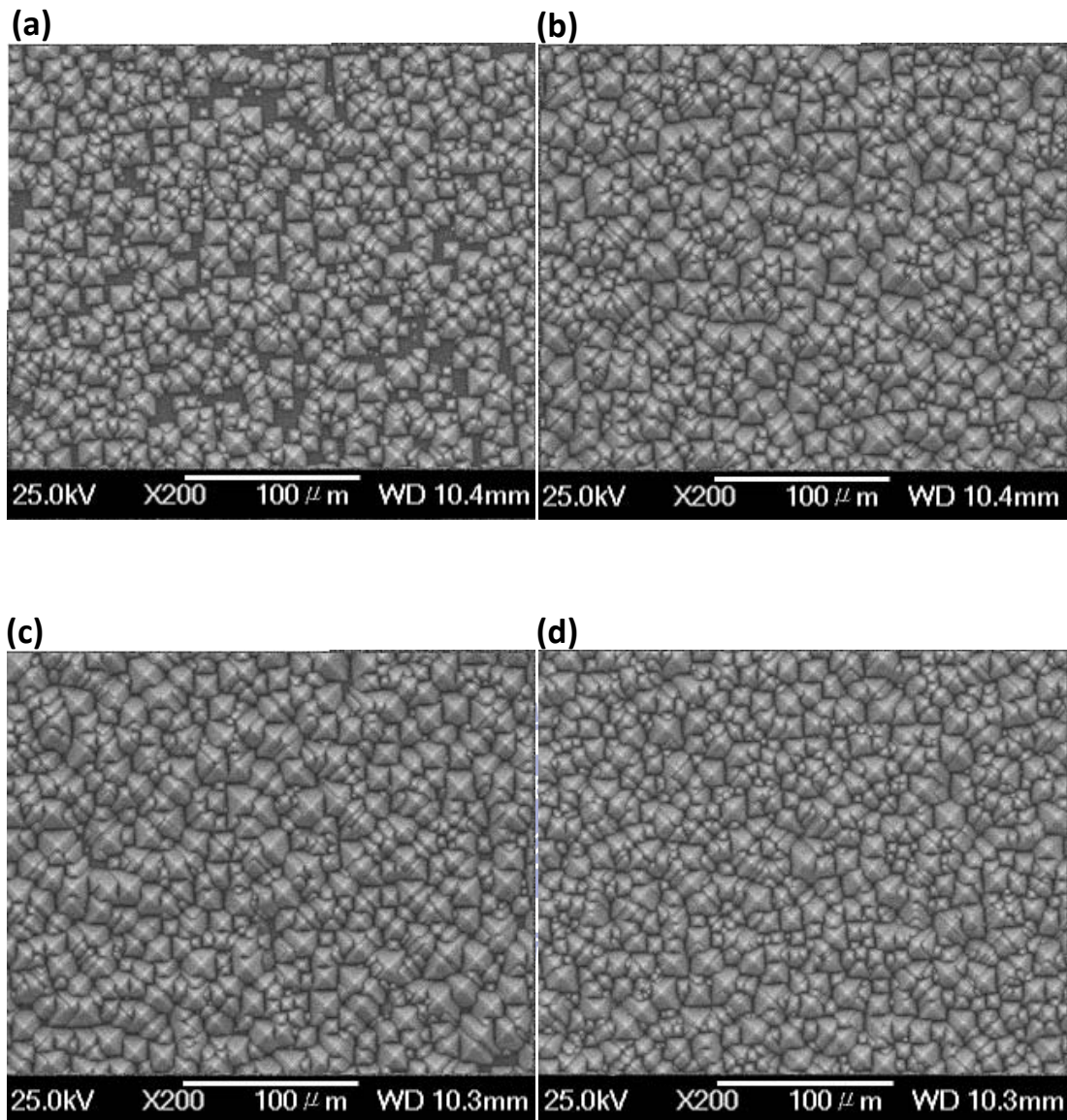


Fig. 2.12: SEM image of silicon surface with different etching time: (a) 30 minutes, (b) 40 minutes, (c) 50minutes, (d) 60minutes.

P-type silicon wafers (100) with a resistivity of 1-10 ohm-cm and *n*-type silicon wafers (100) with a resistivity of 5-10 ohm-cm are used. First, after a standard RCA cleaning process, the surfaces of the wafers are cleaned to remove any organic and

metal impurities. The wafers are dipped in buffed oxide etching (BOE) solution that remove any unintentional oxide after rising the wafers with DI water between each cleaning step. The cleaned wafers are texturized in alkaline etchants using mixtures of potassium hydroxide (KOH) and isopropyl alcohol (IPA) at 85°C. There are five duration times of texturing the surface: 0 minute (polish), 30 minutes, 40 minutes, 50 minutes and 60 minutes as shown in Fig. 2.12. The pyramids of all conditions are 7-10 μm in size. By comparison, the numbers of pyramids at texture time of 30 minutes obvious less and uneven distribution than others as shown in Fig. 2.12 (a).

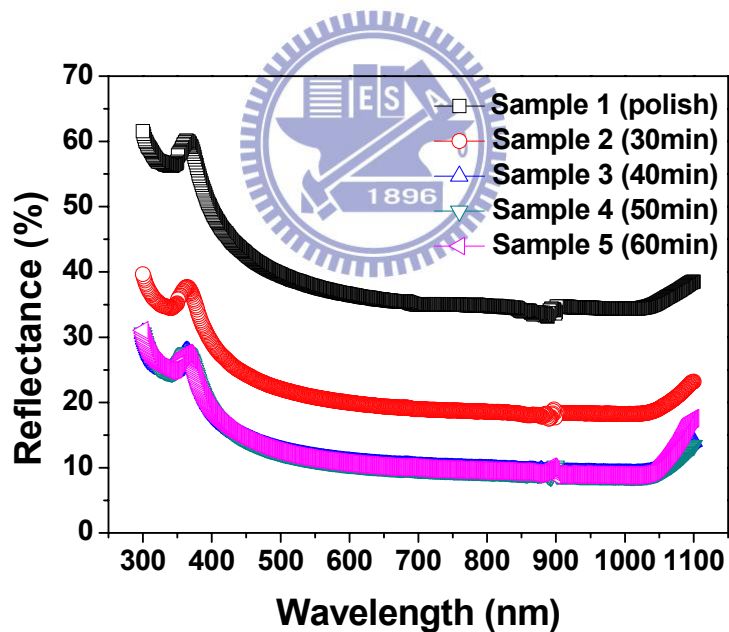


Fig. 2.13: Reflectance of the textured silicon wafers for wavelength between 300 and 1100nm.

Fig. 2.13 shows the surface reflectance with different etching time at wavelengths between 300nm and 1100nm. On the whole, the reflectance of the

non-textured wafer is higher than that of the textured wafers. In addition, the etching time of wafer must exceed 30 minutes, and then, the reflection will close to saturation.

Fig. 2.14 provides a numerical comparison by averaging all of the reflectance values.

These results show that the etching time must exceed 30 minutes to obtain even distribution and lower reflectance of pyramids.

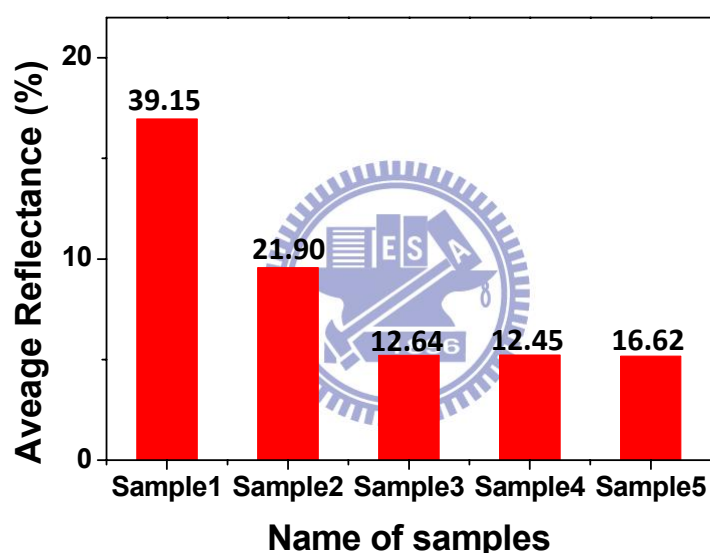


Fig. 2.14: Average % reflectance between 300 and 1100nm.

2.4. Surface Passivation

Crystalline silicon is an indirect semiconductor and hence recombination losses in the material occur largely via defect levels within the bandgap, notably at surface.

Due to the involvement of non-silicon atoms, the situation is more complicated at the silicon surface. The surface represents the largest possible disturbance of the

symmetry of the crystal lattice and hence, because of non-saturated ('dangling') bonds, a large density of defects ('surface states') within the bandgap exists at the surface of the crystal [23].

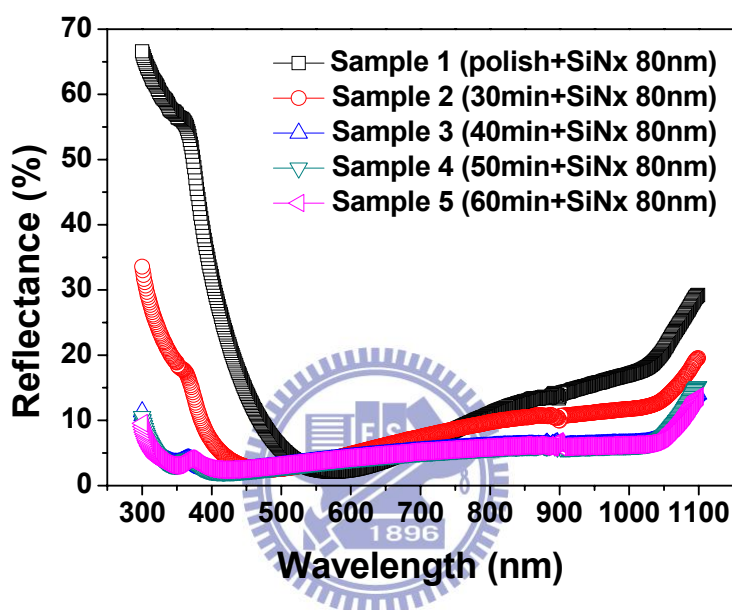


Fig. 2.15: Reflectance of the textured silicon wafers after anti-reflection coating for wavelength between 300nm and 1100nm.

Because of high surface recombination losses and high surface reflectance, the PECVD SiN_x film is deposited on surface as highly efficient surface-passivating and anti-reflection coatings [24-25]. The thickness of 80nm SiN_x is deposited on above substrates (There are five duration times of texturing the surface: 0 minute (polish), 30 minutes, 40 minutes, 50 minutes and 60 minutes) as shown in Fig. 2.13. Compared

with Fig. 2.11, the reflectance is reduced again. Fig. 2.16 provides a numerical comparison by averaging all of the reflectance values. These results show that SiN_x is a good anti-reflection coating layer.

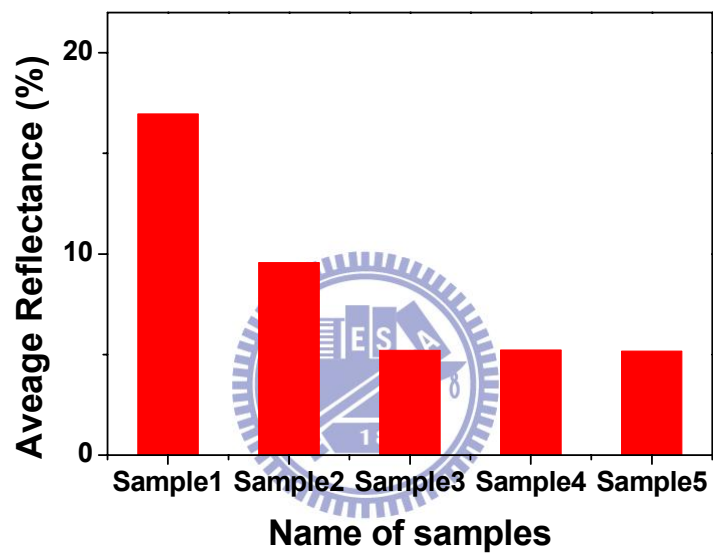


Fig. 2.16: Average % reflectance between 300 and 1100 nm after depositing the SiN_x film.

2.5. Photovoltaic properties of p-type MIS solar cells

In this section, in order to obtain more introduction of light, the semi-transparent metal is removed, textured surface is formed, and then the passivation layer is deposited on top surface as shown in Fig. 2.17

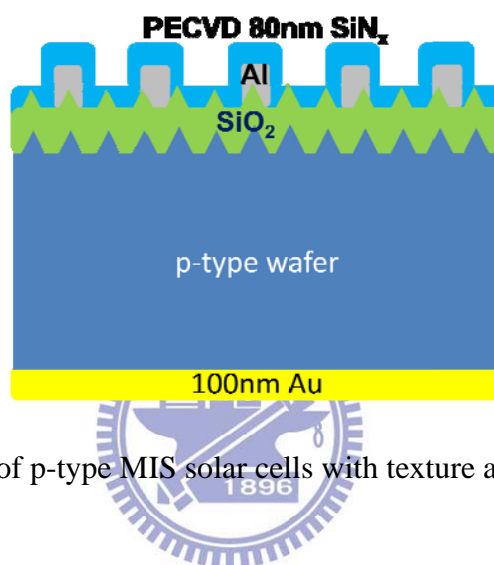


Fig. 2.17: The structure of p-type MIS solar cells with texture and passivation layer.

As shown in Fig. 2.18 with non-textured surface and Fig. 2.19 with textured surface, the J - V curves with SiN_x deposited at 100°C display better photovoltaic properties. From the C-V curve shift (from right (Temp. 300°C) to left (Temp. 100°C)), there are large positive fixed oxide charges within the SiN_x layer at 100°C as shown in Fig. 2.20. It is obvious that the SiN_x film deposited at 100°C can obtain better passivation effect for the MIS solar cells. After the SiN_x film is deposited, not only the current density is improvement outstandingly but the open circuit voltage is also enhanced.

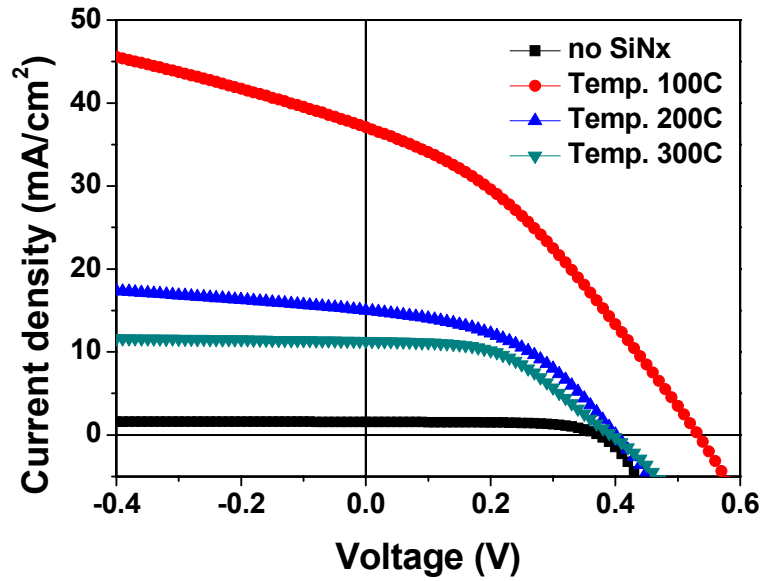


Fig. 2.18: Photovoltaic properties of MIS solar cells after depositing the SiN_x

film with non-textured surfaces.

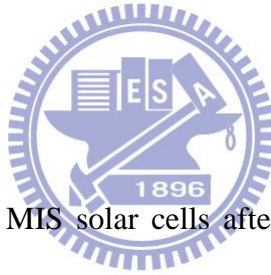


Table 2.2: Photovoltaic of MIS solar cells after depositing the SiN_x film with

non-textured surfaces.

Type	V _{oc} (mV)	J _{sc} (mA/cm ²)	FF (%)	η (%)
No SiN _x (non-texture)	372	1.57	65.75	0.39
100 °C(non-texture)	533	37.07	34.26	6.77
200 °C(non-texture)	400	15.01	43.89	2.64
300 °C(non-texture)	393	11.28	48.16	2.14

The effects of the SiN_x film deposited on the solar cell are ascribed to (i) the reduction of the surface recombination velocity by hydrogen passivation of surface states, (ii) the formation of an inversion layer at the silicon surface by the high positive insulator charges [26] as shown in Fig. 2.20, and (iii) the reduction of surface

reflectance as shown in Fig2.15.

Table 2.2 and Table 2.3 summarize the one-sun parameters of the processed p-type MIS solar cells featuring different surface passivation schemes, as measured under standard testing conditions (25°C , $100\text{mW}/\text{cm}^2$, AM1.5G). The results exhibit significantly enhancement of a short circuit current of $J_{\text{sc}} = 37.07\text{mA}/\text{cm}^2$, an open circuit voltage of $V_{\text{oc}} = 533\text{mV}$ at the condition of 100°C (non-texture).

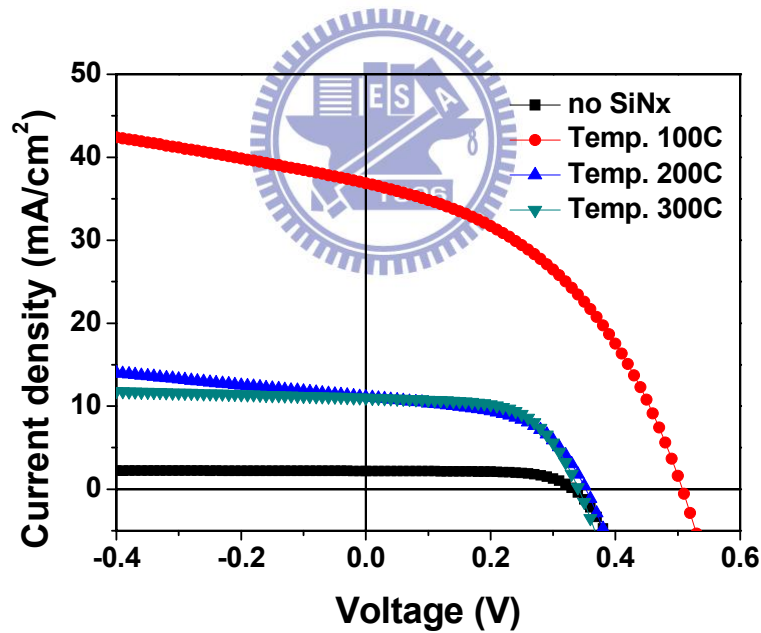


Fig. 2.19: Photovoltaic properties of MIS solar cells after depositing the SiN_x film with textured surfaces.

Table 2.3: Photovoltaic of MIS solar cells after depositing the SiN_x film with

textured surfaces.

Type	V _{oc} (mV)	J _{sc} (mA/cm ²)	FF (%)	η (%)
No SiN _x (texture)	332	2.19	67.1	0.49
100 °C (texture)	507	36.86	42.84	8.01
200 °C (texture)	352	11.10	53.61	2.10
300 °C (texture)	341	11.01	60.09	2.26

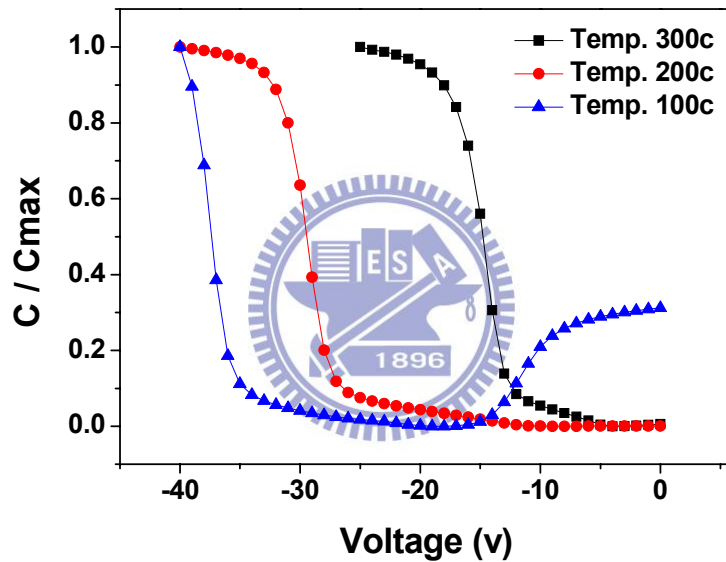


Fig. 2.20: The C-V curve of the SiN_x film with different deposited temperatures.

2.6. Photovoltaic properties of n-type MIS solar cells

The device processes of n-type MIS solar cell are identical as p-type MIS solar cells, except the thickness of SiO₂. Although the SiN_x film is an excellent passivation for p-type MIS solar cells, it is not suitable for n-type MIS solar cells. There are large amount of positive charges within the SiN_x film that can induce an inversion layer in

the p-type silicon underneath the SiN_x . The benefits of the positive charges don't meet requirements of n-type MIS solar cells. Therefore, the Al_2O_3 film by e-gun evaporation is substituted for SiN_x because of the large amount of negative charges within the Al_2O_3 film. We expect that using Al_2O_3 film can induce inversion layer for n-type MIS solar cells applications.

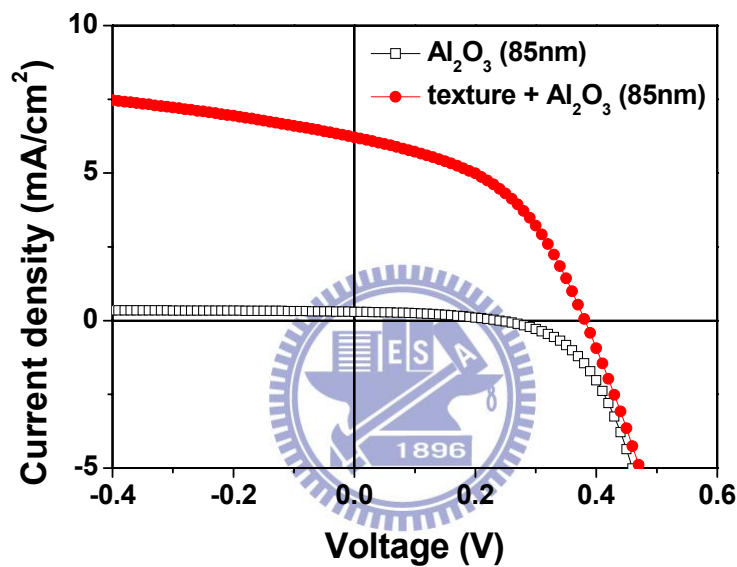


Fig. 2.21: Photovoltaic properties of n-type MIS solar cells with Al_2O_3 films

As shown in Fig.2.21, although there are negative charges within Al_2O_3 film, the effects of the Al_2O_3 film on n-type MIS solar cells are not significantly. From the results, it is probably due to the Al_2O_3 film that is deposited by e-gun evaporating so the quality of the Al_2O_3 film is worse compare with other deposition methods such as ALD [27] and MOCVD. Therefore, the performances of n-type MIS don't get significantly improvement.

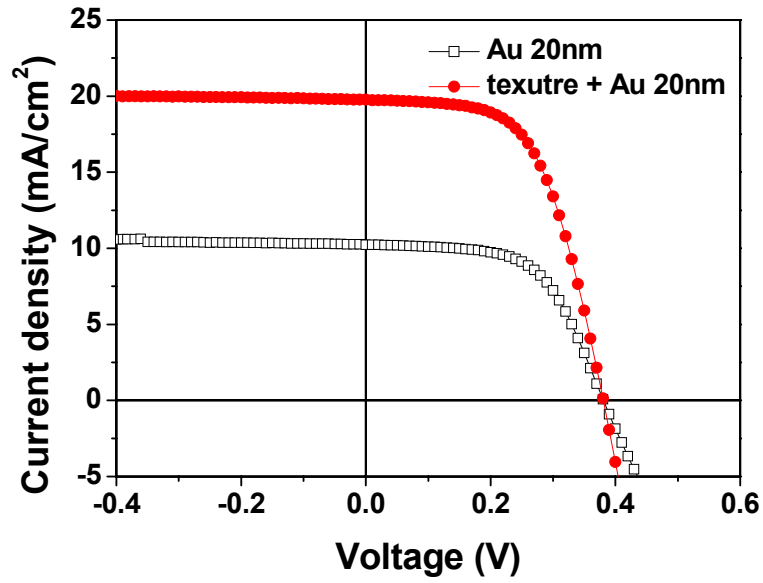


Fig. 2.22: Photovoltaic properties of n-type MIS solar cells with semi-transparent Au

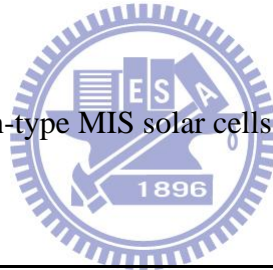


Table 2.4: Photovoltaic of n-type MIS solar cells after depositing Al_2O_3 film or semi-transparent Au

Type	V_{oc} (mV)	J_{sc} (mA/cm^2)	FF (%)	η (%)
Al_2O_3	240	0.3	41.14	0.03
Texture + Al_2O_3	381	6.21	45.49	1.08
Au 20nm	381	10.24	59.43	2.32
Texture + Au 20nm	380	19.76	58.42	4.39

Until now, we don't find the useful passivation layer for n-type MIS solar cells so semi-transparent Au of 20nm is re-deposited on textured surface. Fig. 2.22 shows the J - V curve of n-type MIS solar cells with semi-transparent Au. The summary of the electrical characteristics is shown in Table 2.4.

2.7. Summary

In this chapter, using sputtering SiO_2 as the insulating layer of MIS solar cells has been discussed at different situations. The post annealing in hydrogen atmosphere is necessary because there are a lot of defects in as-deposited sputtering SiO_2 . Moreover, controlling the oxide thickness and working pressure are also critical in MIS solar cells.

To concentrate more incident light, the semi-transparent metal is removed, textured surface is formed, and then the passivation layer is deposited on top surface. Finally, we use the textured surface and the 80nm SiN_x films deposited at 100°C as passivation layer to reduce the surface reflection and the surface recombination. There are exactly improvements in V_{oc} and J_{sc} , but the fill factor is worse. So far, the V_{oc} of MIS solar cells can reach 507mV and 380mV for p-type and n-type on texture surface, respectively.

Chapter 3 MIS stacked solar cells

From the results of chapter 2, the n-type and p-type MIS solar cells are demonstrated, and we use the direct wafer bonding method to combine n-type and p-type in this chapter, then fabricate two MIS solar cells on both side each other. The analysis of the MIS stacked show that the tunneling diode is formed between the n-type and the p-type MIS solar cells, and the total thickness of MIS stacked solar cells is critical.

3.1 Tunneling diode

Tunneling diode is also called Esaki diode [28-30] because it is invented by Leo Esaki in August 1957. It is one of the most important issues affecting performance of stacked solar cell. The effects of the formation of tunnel junction are related to the uniform highly doped layer without defects that result in carrier recombination and leakage currents in depletion regions. In a general tunneling diode, the degenerate semiconductor [31,32] are used to increase tunneling probability via depletion region.

$$E_F - E_v = kT \ln \left(\frac{N_v}{p_0} \right) \quad (\text{Eq. 3.1})$$

$$E_c - E_F = kT \ln \left(\frac{N_c}{n_0} \right) \quad (\text{Eq. 3.2})$$

N_c and N_v are the effective density of states, n_0 and p_0 are doping density of the electron and hole. From Eq. 3.1 and Eq. 3.2, the degenerate semiconductor can obtain

with n_0 and p_0 larger than N_c and N_v .

As shown in Fig. 3.1, the current-voltage characteristics of a tunneling diode are exhibited which is different from traditional p-n junction. The I - V curve shows the ohmic phenomenon at small voltage, and negative differential resistance (NDR) is appeared with increasing forward bias.

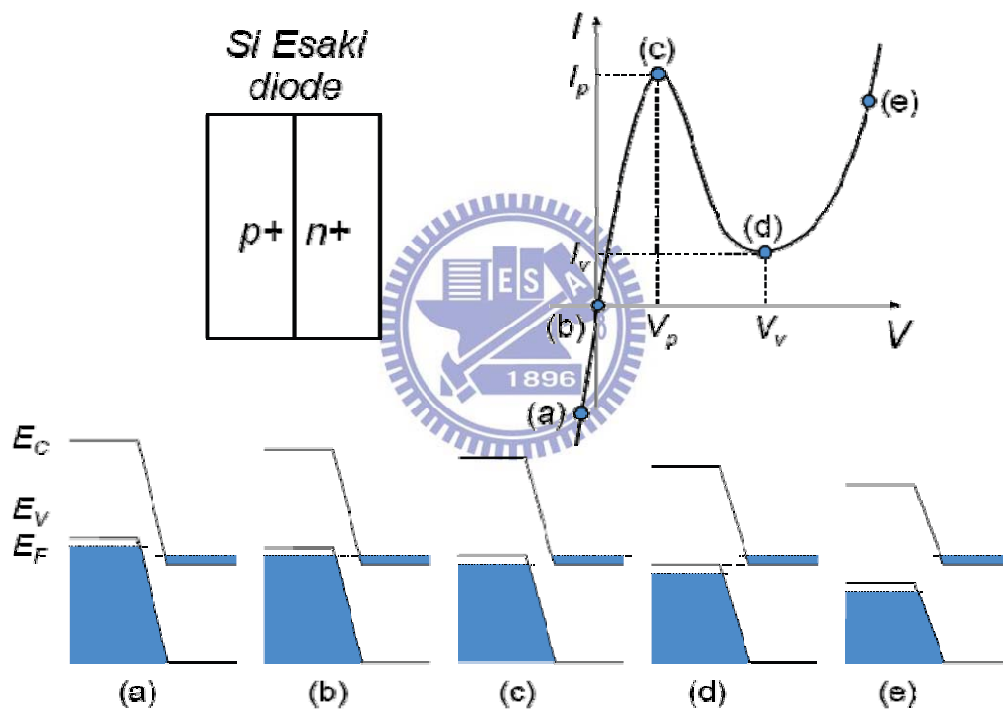
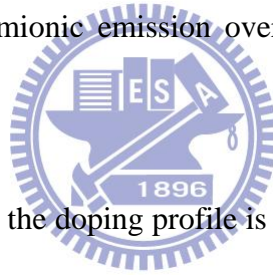


Fig 3.1: Schematic energy band diagram and current-voltage property of tunneling diode with varying bias [33].

The current-voltage characteristics of a tunneling diode can be explained with the I - V characteristic and the band diagram as shown in Fig 3.2 and Fig.3.1. In Fig

3.1(a), when a reverse bias is applied, current flows by electron tunneling from p-side valence band which is occupied states into n-side conduction band which is unoccupied states. In equilibrium, the net tunneling current is zero with no applied bias in Fig 3.1(b). With a small forward bias, current flows by electron tunneling is increased to a peak current I_p at voltage V_p , as labeled in Fig 3.1(c). When the position of conduction band on the n-side is raised above the valence band position on the p-side, the valley current I_v is resulted at a voltage V_v in Fig 3.1(d). With further increasing in the voltage, the current increases due to tunneling through defect states in the depletion layer and thermionic emission over the diode internal barrier, Fig 3.1(e).



For the better performance, the doping profile is key point for the performance in a tunneling diode. Once an abrupt doping profile is obtained, the junction obtains the lower resistance. That is, less voltage loss in a stacked solar cell with a higher V_{oc} could be acquired. On the contrary, the extended profiles of abrupt doping increases the tunneling diode depletion region, and significantly reduces the tunneling probability through depletion region. Accordingly, the performance of stacked solar cell will be dramatically degraded.

Fig.3.2 shows a tunneling junction band diagram with ion implantation on polish sides each other. In order to achieve tunneling diode, a general method is to employ

the doping profile of junction which is hardly control. Therefore, we use direct wafer bonding [34-36] to realize a better tunneling junction between two MIS solar cells.

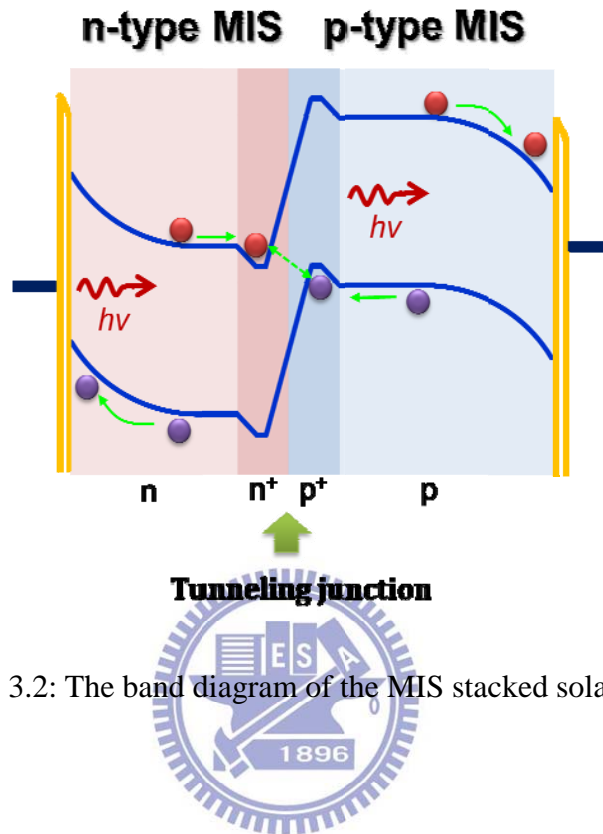


Fig. 3.2: The band diagram of the MIS stacked solar cell

3.2 Fabrication of MIS stacked solar cells

To realize a MIS stacked solar cell, we should integrate three different junctions mentioned in preview sections. 4-inch Si wafers has a thickness about 525um thicker than the skin depth of visible light, so the bottom cell hardly absorbs light under illumination. Due to the prospective of current matching, net current output would be limited by the bottom cell which generates less current. Consequently, before two MIS junction fabrication, a thinning process of bonded pairs must be done to obtain current matching in stacked cells. Chemical etching process is proposed to remove

surface defect and thin the wafer at the same time. Then, using a solution of KOH in IPA, random pyramid is formed on both sides of the stacked cell. The detail processes are listed below and show in Fig. 3.2:

- (1) Wafers are cleaned by RCA clean.
- (2) Ion implantation with dose 5×10^{15} at the polished side.
 - p-side: Energy of implantation are 24KeV and 10KeV.
 - n-side: Energy of implantation are 80KeV and 20KeV.
- (3) Wafers are dipped in dilute HF to remove native oxide.
- (4) Using acetone and IPA to clean by Ultrasonic cleaning.
- (5) Direct bonding of n-type and p-type Si wafers with polished sides each other in IPA and then put the bonded samples into a clamp as shown in Fig. 3.3
- (6) Heat up to 500°C and keep samples at 500°C for 1 hour.
- (7) Dopants activated with rapid thermal annealing (RTA) at 1050°C for 10s.

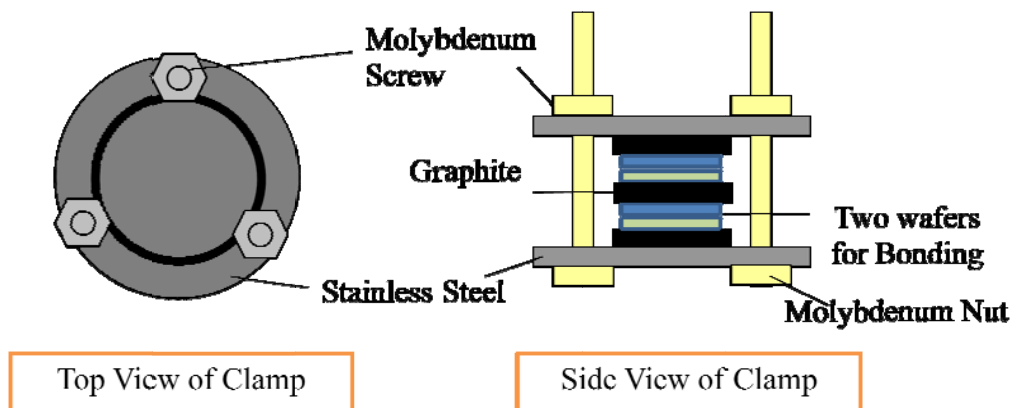


Fig. 3.3: Schematic top view and side view of bonding clamp

- (8) Thinning wafers with Si etchant ($\text{HF}:\text{CH}_3\text{COOH}:\text{HNO}_3=6:7:20$) and texturing wafers with other Si etchant ($\text{KOH}:\text{IPA}:\text{DI water}=1:6:55$).
- (9) Wafers are cleaned by RCA clean.
- (10) Deposit tunneling silicon dioxide with sputter at both sides.
- (11) H_2 annealing at 500°C 1hr for passivating defects in silicon dioxide.
- (12) The top cell deposits the semi-transparent and electrode Au fingers.
- (13) The bottom cell deposits rear electrode Al.
- (14) The structures of MIS stacked solar cells are shown in Fig. 3.3.

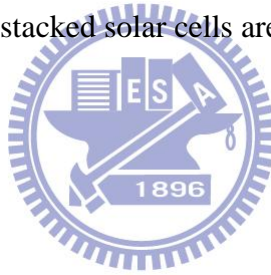


Fig. 3.4: Process flow diagram for the MIS stacked solar cells fabricated.

Fig. 3.5 shows the structure of the MIS stacked solar cell with the 20nm thickness of semi-transparent Au. In order to achieve current matching, after thinning process, the thickness of n-type and p-type become about $90 \mu\text{m}$ and $400 \mu\text{m}$, respectively.

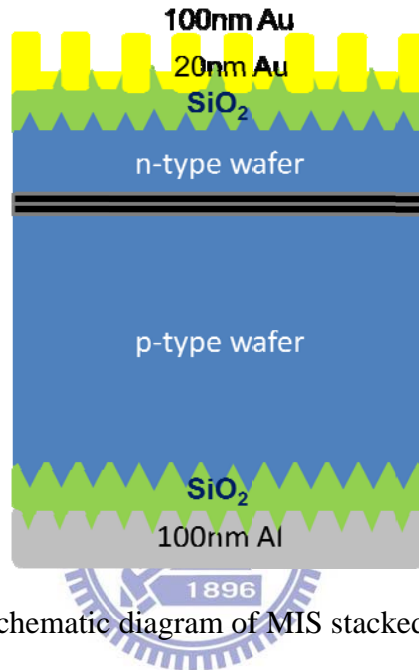


Fig. 3.5: Schematic diagram of MIS stacked solar cells.

3.3 Bonding interface by an IR CCD

In our experiments, all the bonded wafers are commercially available, one side polished, $\langle 100 \rangle$ oriented. All of bonded wafer pairs are inspected by infrared system before and after annealed because the bubbles of bonding interface may occur. The cause of the bubbles form during the stacked cell process include: (1) particles on the bonding surface, (2) localized surface protrusions, (3) localized absence of sufficient density of bonding species, and (4) trapped air pockets [35].

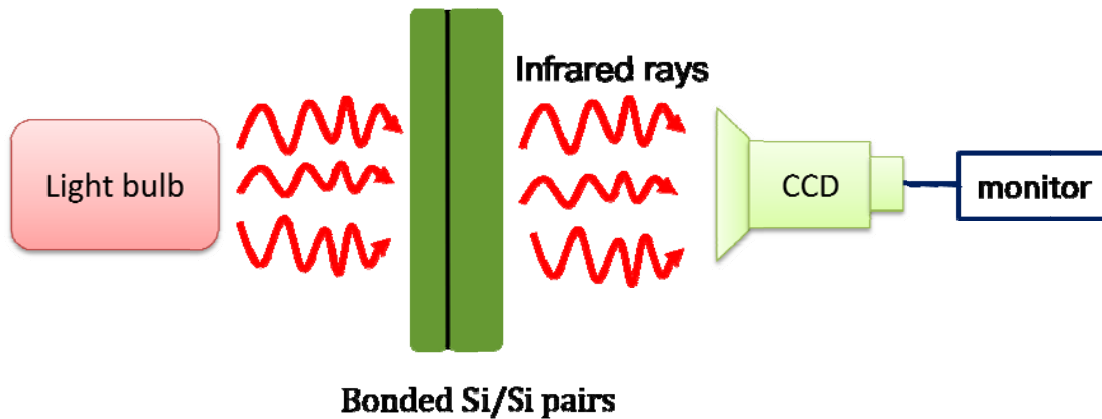


Fig. 3.6: Setup of IR image measurement

Because bonding wafers are not transparent to normal visible light, the transmitting light with an appropriate wavelength based on Eq. 3.3 has to be employed, where E_g is the smaller band gap among the bonding materials if different material are used. According to Eq. 3.3, since crystalline silicon bandgap energy is 1.12eV, only the light with wavelength longer than $1.10 \mu\text{m}$ can pass through crystalline silicon. The light bulb and an IR viewing camera are used to investigate into the imaging system for bonded Si/Si pairs shown in Fig. 3.7

$$\lambda > E_g/h \quad (\text{Eq. 3.3})$$

Fig 3.7 shows that there are four bonding interface images, as Step A, Step B, Step C and Step D, in Fig.3.5. We can find that some certain voids which may cause by above describe are appeared after as-bonded process in Step A. Step B, With RTA

1050°C, the outgassing develops from contaminants on inside bonding materials due to the a heat treatment. Then, Step C, because of RCA clean at 90°C, the gases are diffused along the bonding interface. Finally, when bonded pairs thinning and textured by using silicon etchant, the image don't change obviously because the Step D process temperature of the step D (85°C) is close to Step C.

From the results, if there are a lot of bubbles formed at as-bonded, the bonded Si/Si pairs will easily separate after post processes.

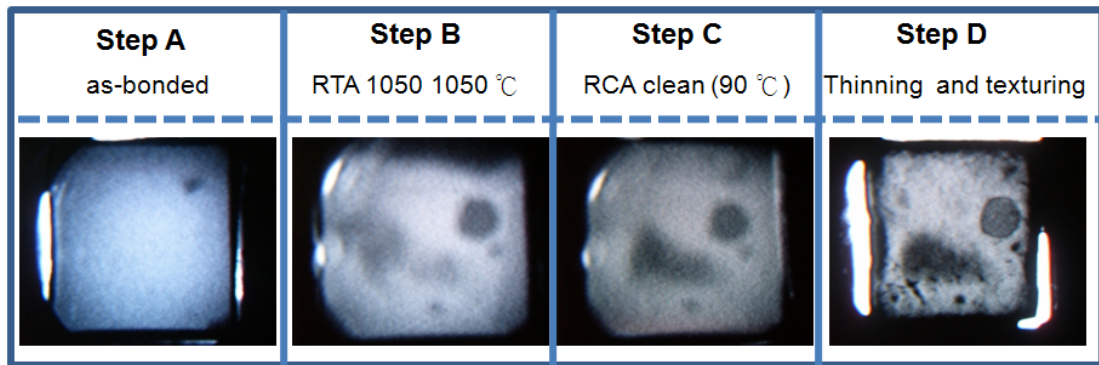


Fig. 3.7: IR images of bonded Si/Si pair in different process Step.

3.4 Photovoltaic properties of MIS stacked solar cells

The current-voltage curves of MIS stacked solar cells under AM1.5 are shown in Fig. 3.8 and Table 3.1. All parameters of the device process are identical unless with or without semi-transparent metal. The cell is thinning as above describe, the thickness of n-type and p-type are about $90 \mu\text{m}$ and $400 \mu\text{m}$, respectively. From the currents of Fig 3.8, J_{sc} is low about $5.9\text{mA}/\text{cm}^2$ despite with or without semi-transparent metal.

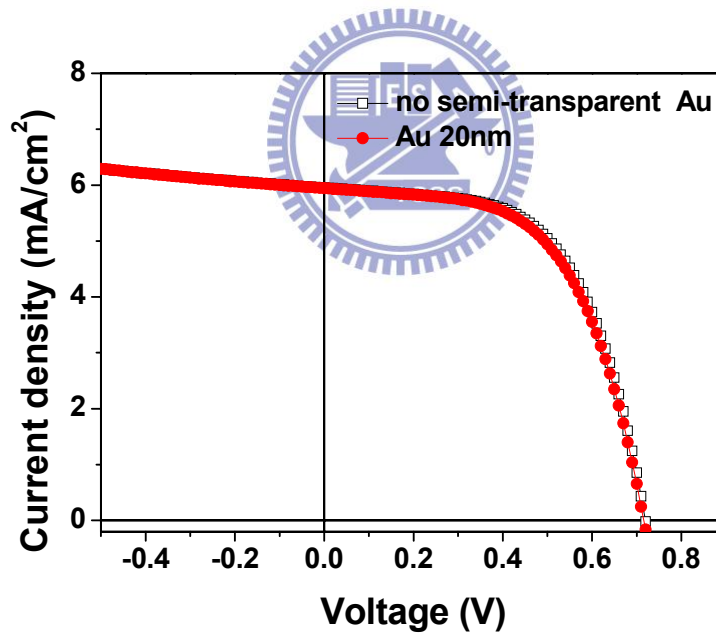


Fig. 3.8 Photovoltaic properties of MIS stacked solar cells with or without semi-transparent metal.

Table 3.1 Photovoltaic properties of MIS stacked solar cells with and without semi-transparent metal.

Type	V_{oc} (mV)	J_{sc} (mA/cm ²)	FF (%)	η (%)
No semi-transparent Au	720	5.96	58.96	2.53
Au 20nm	716	5.94	58.04	2.47

Through the incident photon to current efficiency (IPCE) curves as shown in Fig. 3.9, we can realize J_{sc} by IPCE measurement system are higher than solar simulator measurement system, and the currents with semi-transparent metal cell are larger than without semi-transparent metal cell. In Table 3.2, The semi-transparent metal improve the currents of IPCE measurement but the currents have no enhancement of solar simulator measurement systems which ascribe to limited current by the bottom cell.

Table 3.2: The current density is measured by different measurements (solar simulator and IPCE).

Type	Solar simulator J_{sc} (mA/cm ²)	IPCE J_{sc} (mA/cm ²)
no semi-transparent Au	5.96	9.55
Au 20nm	5.94	12.48

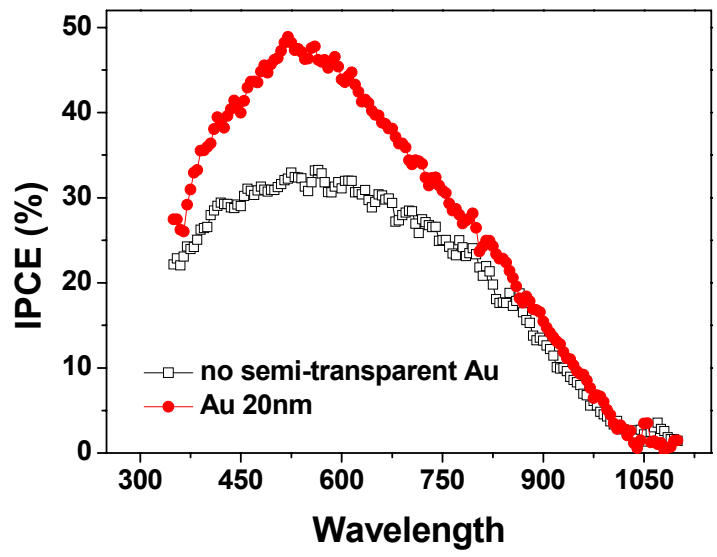


Fig. 3.9: IPCE curves of MIS stacked solar cells with and without semi-transparent metal.

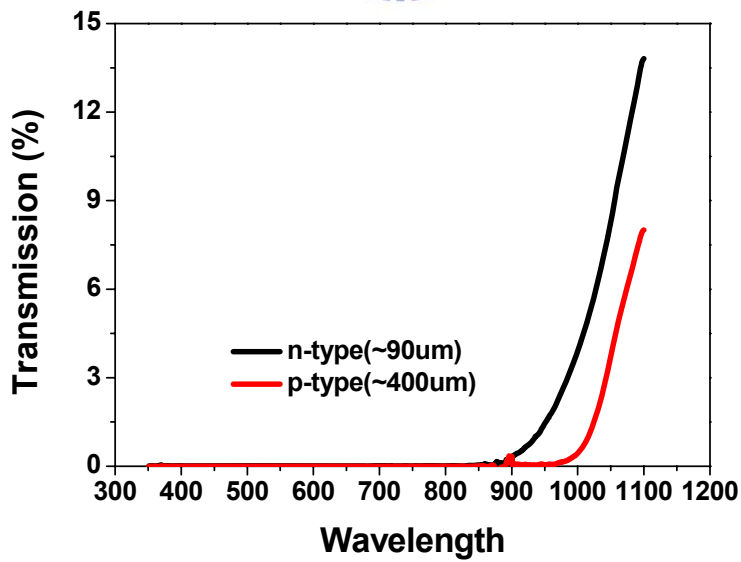


Fig. 3.10: The transmission of different wafer thickness.

However, we can realize that the transmission of the thickness $90\ \mu\text{m}$ of n-type silicon increase drastically after an appropriate 900nm of wavelength from the Fig. 3.10. It means that the bottom cell would absorb infrared light not the visible light so the photo currents of bottom cell would be small.

3.5 Summary

The tunneling diode is fabricated by direct bonding method with ion implantation on polish side each other. Dopants are activated by RTA at 1050°C . In order to get current matching, the thickness of devices has to thinning by silicon etchants. Although the total thickness are reduced to $490\ \mu\text{m}$, the device are not transparent to normal visible light, the transmitting light with an appropriate wavelength is 900nm . The bottom cell absorbs too less light, so products a little current. Finally, we integrate the n-type and the p-type to form a MIS stacked solar cell which can obtain $V_{oc}=720\text{mV}$, $J_{sc}=5.96\text{mA}/\text{cm}^2$, $\text{FF}= 58.96\%$, $\eta = 5.93$. The V_{oc} of MIS stacked cells obtain 720mV which is larger than that of p-type and n-type cells.

Chapter 4 Conclusion and future work

4.1 Conclusion

In this study, first, the characteristics of both p-type and n-type Metal-Insulator-Semiconductor (MIS) solar cells with sputtering SiO₂ insulating layers fabricated by radio-frequency (RF) magnetron sputtering are investigated individually.

From the beginning, the structure of the MIS solar cell is proposed with the semi-transparent metal on both n-type and p-type silicon substrates. The influence of processes parameters are researched such as H₂ annealing, insulating layer thickness and the working pressure on the MIS solar cell. However, the reflection of surface is high due to the semi-transparent metal. In order to reduce the reflection of surface, we remove the semi-transparent metal, form the texture on surface, and then deposit the passivating SiN_x film on surface as a AR coating which also can induce the inversion layer on the insulating layer between metal and semiconductor so that improve the performance of the p-type MIS solar cells. Regarding the n-type MIS solar cells, we also deposit Al₂O₃ film as the passivating layer, but the effects on n-type MIS solar cell are not obviously. Therefore, the structure of n-type MIS solar cells with the semi-transparent metal are used to make the MIS stacked solar cell. So far, MIS solar cells reach V_{oc} 380mV and 507mV with n-type and p-type silicon wafer, respectively.

Finally, by the direct wafer bonding, we integrate the n-type and the p-type to form a MIS stacked solar cell which can obtain $V_{oc}=720\text{mV}$, $J_{sc}=5.96\text{mA}/\text{cm}^2$, $\text{FF}=58.96\%$, $\eta = 5.93$. The V_{oc} of MIS stacked cells obtain 720mV which is larger than that of p-type and n-type cells.

4.2 Future work

Although the V_{oc} on the MIS stacked solar cell is 720mV which is lower than theoretic V_{oc} equals to 0.9V . There are still many issues that exist in the staked cell. The voltage drops at the bonding interfaces that can further improve by the tunneling current with proper dopants activation and defect passivation. However, the total thickness of MIS stacked solar cell is another important issue. In order to obtain the current matching, the bottom cell needs to absorb more sunlight. Therefore, the total thickness has to be decreased and optimized.

In addition to the issues of the bonding interface and thickness, we can use different substrate to bond together such as Ge substrate, or deposit different bandgap Si such as uc-Si so that in order to absorb different region sunlight. Although the semi-transparent metal has been removed, the finger electrodes also reflect the sunlight. The transparent conductive oxide such as ITO and ZnO can be introduced in the stacked solar cell with the aid of sputtering to further increase J_{sc} .

References

- [1] Zhores I. Alferov, V. M. Andreev, M. B. Kagan, I. I. Protasov, and V. G. Trofim, Fiz. Tekh. Poluprovodn, Vol.4 ,p.2378 (1970)
- [2] Zhores I. Alferov, Rev. Mod. Phys., Vol.73, p.767 (2001)
- [3] R. Hezel, Prog. PV Res. Appl. ,Vol.5, p.109 (1997)
- [4] R. Hezel, Solid State Electron., Vol.24, p.863 (1981)
- [5] R. Hezel and R. Schorner, J. Appl. Phys., Vol.52, p.3076 (1981).
- [6] R. Schorner and R. Hezel, IEEE Trans. Electron. Devices, ED-28, p.1466 (1981)
- [7] R. Hezel, Conf. Rec. 16th IEEE Photovoltaic Specialists Conf., San Diego, p.1237 (1982)
- [8] K. Jaeger and R. Hezel, IEEE Trans. Electron. Devices, ED-32, p.1824 (1985)
- [9] R. Hezel, W. Hoffmann and K. Jaeger, Proc. 10th European Photovoltaic Solar Energy Conf., Lisbon, p. 511 (1991)
- [10] A Metz, R Meyer, B Kuhlmann, M Grauvogl and R Hezel , Proceedings of the 26th IEEE PVSC, p.31 (1997)
- [11] Kuo-Chung Lee and Jenn-Gwo Hwu, IEEE Electron Device Lett., Vol.18, p.565 (1997)
- [12] Chih-Yao Wang and Jenn-Gwo Hwu, J. Electrochem. Soc., Vol.156, p.3 (2009)
- [13] Manfred Grauvogl, Armin G. Aberle, and Rudolf Hezel, Appl. Phys. Lett., Vol.69,

p.69 (1996)

[14] Armin G. Aberle and Rodolf Hezel, Prog. Photovoltaics., Vol.5, p.29 (1997)

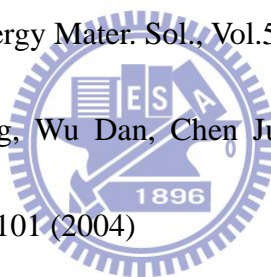
[15] A. Hartstein and D. R. Youn, Appl. Phys Lett., Vol.38, p.631 ()

[16] Asuha, Y-L Liu, O. Maida, M. Takahashi, and H. Kobayashi, J. Electrochem. Soc., Vol.151, p.G824 (2004)

[17] P.K. Singh, R. Kumar, M. Lal, S.N. Singh, B.K. Das, Sol. Energy Mater. Sol., Vol.70, p.103 (2001)

[18] E. Vazsonyi, K. De Clercq, R. Einhaus, E. Van Kerschaver, K. Said, J. Poortmans, J. Szlufcik, J. Nijs, Sol. Energy Mater. Sol., Vol.57, p.179 (1999)

[19] Zhenqiang Xi, Deren Yang, Wu Dan, Chen Jun, Xianhang Li, Duanlin Que, Renew. Energy, Vol.29, p.2101 (2004)



[20] Hayashi Shota, Minnemoto Takashi, Takakura Hideyuki, Hamakawa Yoshihiro, Rare Metals, Vol.25, p.115 (2006)

[21] David L. King, M. Elaine Buck, p303 IEEE (1991)

[22] J.W. Faust Jr., E.D. Palik, J. Electrochem. Soc., Vol.130, p.1413 (1983)

[23] Armin G. Aberle, Prog. Photovoltaics., Vol.8, p.473 (2000)

[24] Hayoung Park, Soonwoo Kwon, Joon Sung Lee, Hee Jin Lim, Sewang Yoo and Donghwan Kim, Sol. Energy Mater. Sol., Vol.93, p.1773 (2009)

[25] Hayoung Park, Joon Sung Lee, Soonwoo Kwon, Sewang Yoo and Donghwan

- Kim, Curr. Appl. Phy., Vol.10, p.113 (2010)
- [26] E.P. Burte and R.Hezel, J. Appl. Phys., Vol.55, p.4 (1984)
- [27] J.Schmidt, A.Merkle, R. Brendel, B. Hoex, M. C. M. van de Sanden and W. M. Kessels, Prog. Photovolt: Res. Appl., Vol.16, p.461 (2008)
- [28] L. Esaki, Phys. Rev., Vol.109, p.603 (1958)
- [29] L. Esaki, Proc. IEEE, Vol.62, p.825 (1974)
- [30] L. Esaki, IEEE Transactions on Electron Devices, Vol. ED-23, p.644 (1976)
- [31] S. M. Sze, “Physics of Semiconductor Devices” 2nd Ed. (Wiley, New York, 1981)
- [32] DA Neamen, “Semiconductor Physics and Devices” 3rd Ed. (McGraw-Hill, New York,2003)
- [33] Y Yan, “SILICON-BASED TUNNEL DIODE TECHNOLOGY”
- [34] Xuan Xiong Zhang and Jean-Pierre Raskin, J. Microelectromech. Syst., Vol.14 p.2 (2005)
- [35] Q-Y. Tong and U.Gosele, “Semiconductor Wafer Bonding: Science and Technology ”
- [36] Seiji Fujino, Masaki Matsui, Tadashi Hattori and Yoshihiro Hamakawa, Jap. J. Appl. Phys., Vol.34, p.L1322 (1995)

